Journal of Volcanology and Geothermal Research 385 (2019) 179–197

Contents lists available at ScienceDirect

Journal of Volcanology and Geothermal Research

journal homepage: www.elsevier.com/locate/jvolgeores

Telkibánya lava domes: Lithofacies architecture of a Miocene rhyolite field (Tokaj Mountains, Carpathian-Pannonian region, Hungary)

János Szepesi[a,b,*], Réka Lukács[a], Ildikó Soós[a], Zsolt Benkó[b], Zoltán Pécskay[b], Zsuzsanna Ésik[c], Miklós Kozák[c], Andrea Di Capua[d], Gianluca Groppelli[d], Gianluca Norini[d], Roberto Sulpizio[d,e], Szabolcs Harangi[a,f]

[a] MTA-ELTE Volcanology Research Group, Budapest, Hungary
[b] Isotope Climatology and Environmental Research Centre (ICER), Institute for Nuclear Research, Hungarian Academy of Sciences, Debrecen, Hungary
[c] University of Debrecen Department of Mineralogy and Geology, Debrecen, Hungary
[d] Istituto di Geologia Ambientale e Geoingegneria, Consiglio Nazionale delle Ricerche, Milano, Italy
[e] Dipartimento di Scienze della Terra e Geoambientali, Università degli Studi di Bari, Bari, Italy
[f] Department of Petrology and Geochemistry, Eötvös University, Budapest, Hungary

ARTICLE INFO

Article history:
Received 26 November 2018
Received in revised form 4 June 2019
Accepted 4 July 2019
Available online 5 July 2019

Keywords:
Lava dome/flow stratigraphy
Lithofacies analysis
Rhyolite
Perlite
Emplacement

ABSTRACT

This work focuses on the Miocene Telkibánya Lava Dome Field (Tokaj Mountains, Hungary), proposed as an example of poorly investigated lithofacies architecture of old silicic lava dome fields. A detailed fieldwork, combined with petrographic and radiometric (K/Ar dating) analyses, allows us the redefinition of the volcano-stratigraphy of a 25 km^2 area, and the recognition of two temporary different generation of domes that grew in a subaerial environment. 12 cohesive and autoclastic lithofacies are identified and grouped together to document the internal variability of the domes, as well as the erosional phases that affected the lithofacies architecture. Furthermore, stratigraphy, lithofacies association and morphology allow recognizing the areal distribution of 5 lithosomes (lava flows, coulées or domes). All these findings represent a major breakthrough in the identification and interpretation of the volcanic processes that control the growth of silicic lava domes and their products in Late Miocene environment of Carpathian Pannonian region.

1. Introduction

Rhyolitic volcanic edifices are generally represented by highly viscous, thick (up to 100 m), small-volume (<1 km^3) domes and associated short (less than a few kilometres) lava flows (Fink, 1983; Stevenson et al., 1994a, b; Bullock et al., 2018). Their emplacement is often connected to dome fields or to large caldera-forming explosive eruptions at the early and/or late stages of silicic eruption cycles (Taylor Creek, New Mexico – Duffield et al., 1995; Mono-Inyo Field –Hildreth, 2004; Rotorua, New Zealand – Ashwell et al., 2013). Internal architecture of lava flows and domes have been characterized in the field and through descriptive textural approaches (e.g. fragmentation types, groundmass vesicularity, crystallinity) both on young lava flows and domes (Inyo Domes: Manley and Fink, 1987; Fink and Manley, 1987; Big Obsidian Flow, Castro et al., 2002; Puyehue-Cordon Caulle, Tuffen et al., 2013; Rocce Rosse, Shields et al., 2016; Bullock et al., 2018; Taupo Volcanic Zone, Stevenson et al., 1994a, b) and old dome examples (Calico Hills Formation, Christiansen and Lipman, 1966; Sweetkind and Bova, 2015; Paranà Magmatic Province, Polo et al., 2018; Carpathian Pannonian Region, Lexa et al., 2014; Németh et al., 2008; Seghedi, 2011; Rhodopes, Bulgaria Dhont et al., 2008). Nevertheless, detailed comparisons among facies architectures and textural characteristics between the edifices of ancient and modern volcanic environments are missing for a better comprehension of the emplacement processes controlling silicic dome growth and volcanic eruptions.

This paper aims to fill this gap, unravelling the lithofacies architecture of the Telkibánya Lava Dome Field (TLDF) succession of the north-eastern part of the Carpathian-Pannonian Region (eastern-central Europe) evolved during the Late Miocene (Fig. 1). Through combinations of detailed geological mapping, lithofacies analysis in the field and at petrographic scale, and new radiometric data (K/Ar dating), a reconstruction of the TLDF stratigraphy and the flow/dome architecture of 5 different volcanic lithosomes grown during two volcanic stages are provided, proposing the identi-

* Corresponding author at: MTA-ELTE Volcanology Research Group, 1117 Pázmány Péter Sétány 1/c, Budapest, Hungary.
E-mail address: szepeja@gmail.com (J. Szepesi).

https://doi.org/10.1016/j.jvolgeores.2019.07.002
0377-0273/

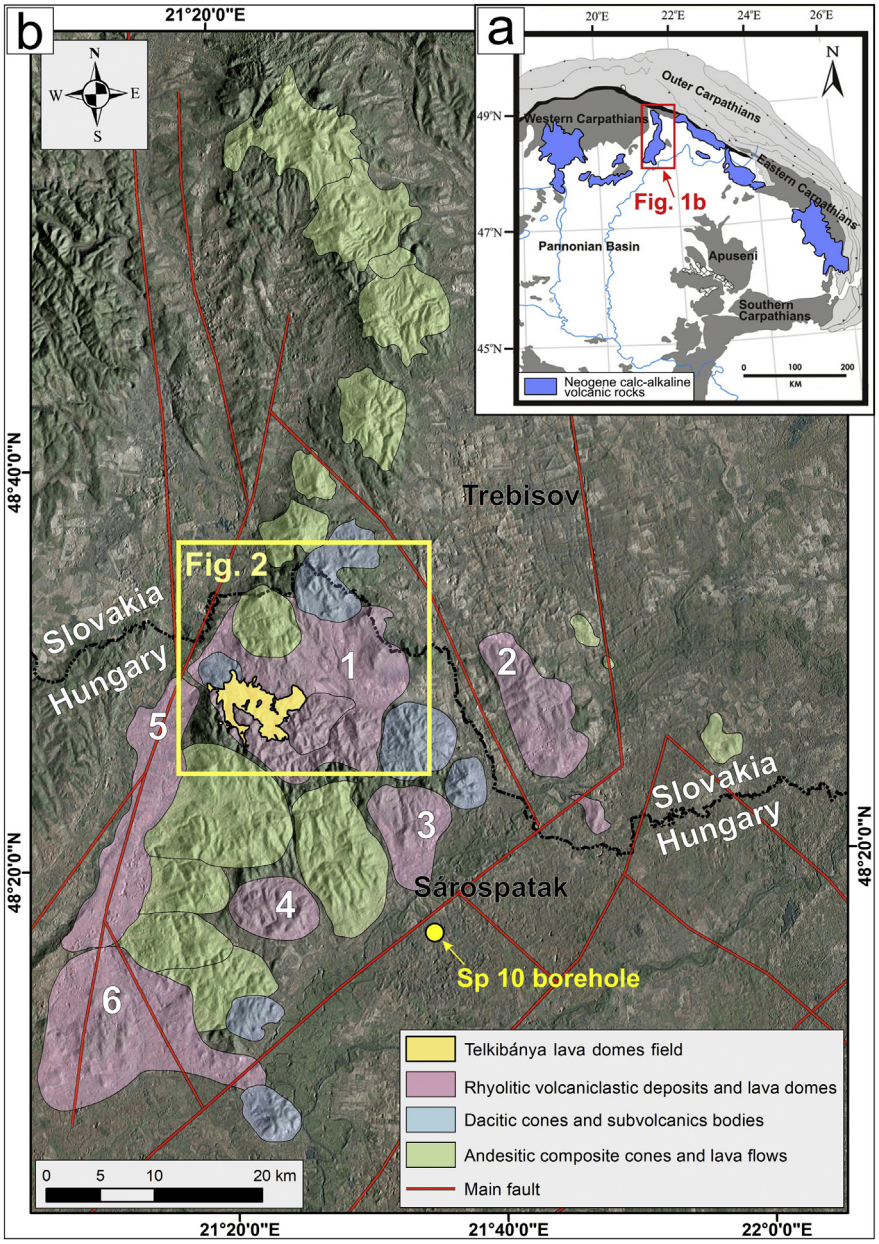

Fig. 1. Major volcanic centres and tectonic lineaments of the Tokaj-Slanske Mountains. Silicic centres (white): 1. Telkibánya-Pálháza volcaniclastics and lava domes (see on Fig. 3), 2. Zemplin volcaniclastics and lava domes, 3. Megyer-Király Hill volcaniclastics (Badenian), 4. Szokolya – Nagy Páca lava dome group, 5. Vizsoly volcaniclastics and lava domes, 6. Szerencs caldera volcaniclastics and lava domes. A) Location of Tokaj-Slanske Mountain in the Carpathian–Pannonian Region (blue areas show Neogene calc-alkaline volcanic rocks on the surface). Yellow square indicates the location of Fig. 2. Data from Kaličiak and Žec (1995); Zelenka et al. (2012). Digital elevation map: SRTM Data (Shuttle Radar Topography Mission, https://lta.cr.usgs.gov/SRTM1Arc.). (For interpretation of the references to colour in this figure legend, the reader is referred to the web version of this article.)

fication and interpretation of silicic volcanic products and their emplacement processes.

2. Geological background

The TLDF is included in the Tokaj-Slankse Mountains (TSM - Fig. 1), a north-south trending, arcuate, Miocene volcanic chain developed in a 15–25 km wide, faults aligned graben-like structure (Gyarmati, 1977; Kaličiak and Žec, 1995; Zelenka et al., 2012). This volcanic chain extends over 100 km through the Hungarian-Slovakian border roughly perpendicular to the orogenic belt of the Carpathians. Repeated andesitic to rhyolitic volcanic eruptions took place from ca. 15 to 10 Ma (Pécskay et al., 1987, 2006; Pécskay et al., 1995; Pécskay and Molnár, 2002). The biostratigraphy confirms the transitional shallow marine to subaerial environment (Central Parathetys NN 5–7 biozone, Szentgyörgyi, 1978; Kováč et al., 2007, 2018; Piller et al., 2007). The volcanic landforms (Kaličiak and Žec, 1995; Lexa et al., 2010; Zelenka et al., 2012; Fig. 1) consist of caldera systems, rhyolitic lava dome fields and andesitic composite volcanoes. The total thickness of the volcanic deposits is estimated to exceed the 2000 m according to geophysical data (Zelenka et al., 2012). Major element data indicates the dominance of intermediate (SiO_2 = 56–63%) and high-silica (SiO_2 = 75%<) suites, whereas a basaltic dyke was described from a drilling (for location, see Fig. 1) and represents the latest stage of volcanism (Downes et al., 1995; Kiss et al., 2010).

The investigated area is included in the middle part of the TSM (Fig. 2), where rhyolitic calc-alkaline volcanism occurred from

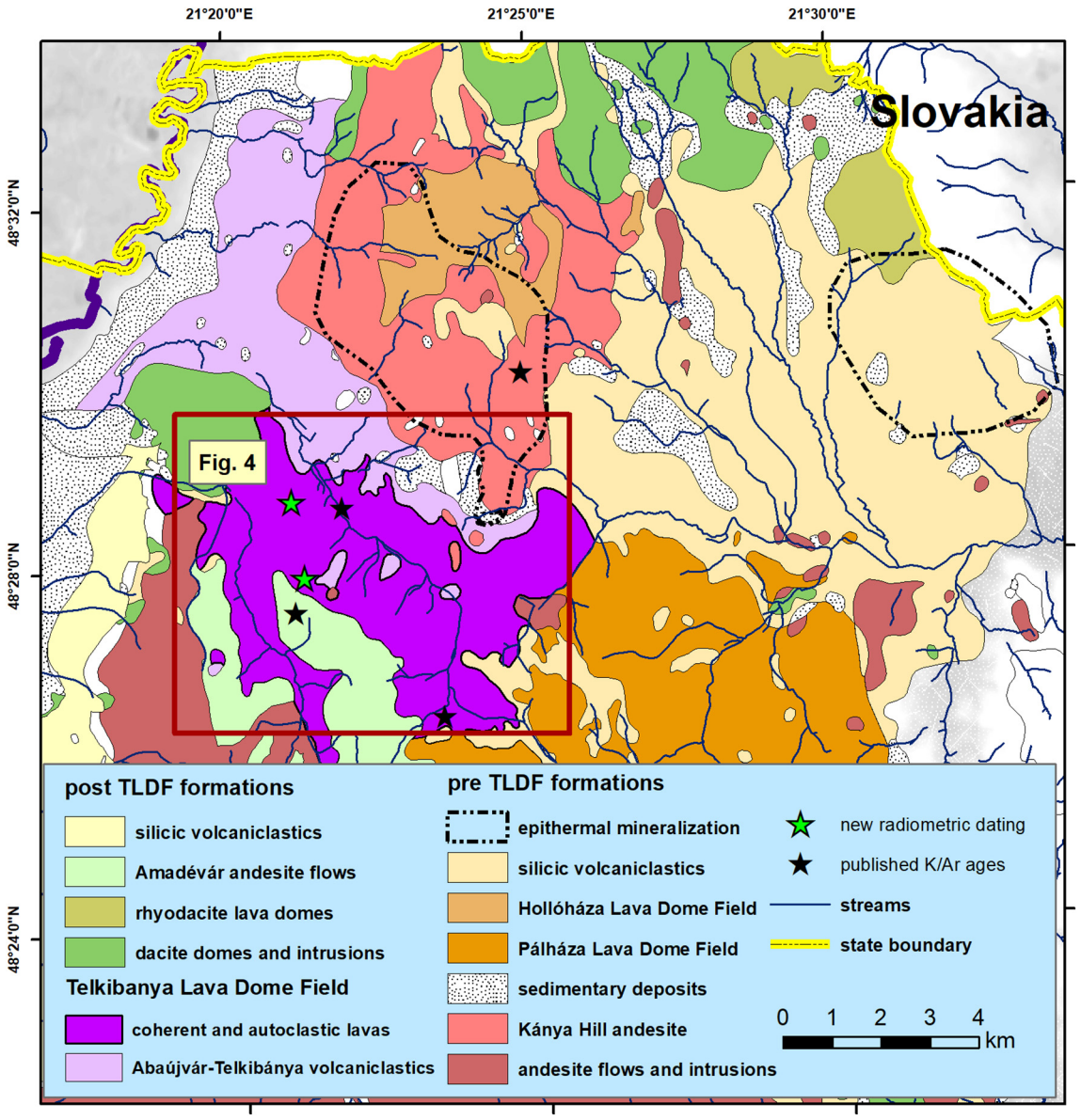

Fig. 2. Geological map of the Telkibánya Lava Dome Field area (TLDF) (13.9–11.2 Ma, see Table 2) in the middle part of the Tokaj-Slanske Mountains. Red square indicates the location of Fig. 4. Data compiled from Ilkey-Perlaki (1971, 1977). (For interpretation of the references to colour in this figure legend, the reader is referred to the web version of this article.)

13.6 ± 0.5 Ma to 11.2 ± 0.7 Ma (Pécskay et al., 1987; Kiss et al., 2010; Zelenka et al., 2012). Volcaniclastics and lavas cover ca. 250 km^2 (Fig. 2) with a maximum thickness of 500 m (Ilkey-Perlaki, 1972). The stratigraphic scheme has been established during geological mapping (Ilkey-Perlaki, 1967, 1971, 1977, 1978) and perlite exploratory drilling projects (Ilkey-Perlaki, 1972; Gyarmati, 1981) of the '60–'80. These studies defined the main regional sedimentary and volcanic (both explosive and effusive) units and identified the submarine to subaerial transition of the volcanism. Regionally four main units have been identified, from top to bottom: clay and marine sediments, followed by unwelded to partially welded and redeposited rhyolitic tuff, by rhyolitic lava domes and, at the top, by andesitic lava flows (Kiss and Zelenka, 2009). Unfortunately, the published data provide limited information for a detailed volcanological reconstruction. Recently few volcanological studies have been published related to the study area. Németh et al. (2008) and Zelenka (2013) describe structures, facies, evolution and emplacement processes of the submarine Pálháza Lava Dome complex. Moreover Lexa et al. (2014) characterize a complex evolution of the rhyolitic Viničky volcano along the Hungarian-Slovakian border. However none of these papers discusses the facies architecture of the subaerial effusive rhyolitic volcanism in the region.

3. Methods

A detailed field work on the TLDF was carried out in order to 1) redefine the volcano-stratigraphy of the area, and 2) to document the lithofacies variations of the silicic dome/flow bodies. In addition to the field data (about 40 logs), the stratigraphy of 35 boreholes for ore geology exploration published by Ilkey-Perlaki (1967, 1972, 1978) and Gyarmati (1981) have been also revised and correlated to the fieldwork results to obtain a wider knowledge of the 3D volcanic bodies distribution in the poorly exposed areas.

The fieldwork investigation at TLDF has been performed using lithostratigraphic units (Salvador, 1994; Groppelli and Martí, 2013; Martí et al., 2018), allowing the recognition of both volcanic and non-volcanic formations. To define lithostratigraphic units we have applied continuity correlation of individual lithofacies zones in

Table 1
Descriptive textural markers of silicic lava lithofacies zones and related emplacement processes.

Feature	Related process	Main marker	Lithofacies association
Vesicle pore structure	*Vesiculation*	Connected Individual	Lapilli tuffs, carapace breccia Transition zone, microcrystalline core
Vesicle size	*Vesiculation, devitrification*	Fine (<mm) Medium (mm-cm) Coarse (cm<)	Lapilli tuffs, carapace breccia Transition zones, microcrystalline core
Grain size distribution	*Quench or explosive fragmentation*	Matrix supported Clast supported Sorted Unsorted	Lapilli tuffs Carapace breccia Fallout deposits Lapilli tuffs, carapace breccias
Lithoclast size	*Quench or explosive fragmentation*	Coarse grained (dm<) Medium (<dm) Fine grained (cm)	Lapilli tuffs, carapace breccia, basal breccia
Clast alignment	*Welding*	Jig-saw fit Clast rotated Flattened	Carapace, internal, basal breccia
Perlitic fracturing	*Hydration*	Weak Dense	Carapace breccia, coherent glass
Flow banding pattern	*Lava flowage*	Planar *Meso* scale folding Chaotic	Coherent glass, transition zone, microcrystalline core
Flow banding angle	*Flow/dome structure, folding*	Low angle (<30°), Moderate (30–60)° High angle (60°>)	Independent variable
Spherulites	*Devitrification*	Large (cm-dm) Small (<cm)	Transition zone microcrystalline core
Lithophysae		Lithophysae	
Groundmass crystallinity	*Groundmass crystallization*	Felsitic Granophyric Axiolithic Poikilitic	Transition zone microcrystalline core

different outcrops in addition to the classical lithological and stratigraphic features (de de Vita et al., 2010). The horizontal and vertical correlations of volcanic bodies allowed recognizing some effusive centers related to lava flows and domes. In these cases, we adopted lithosomatic units (Salvador, 1994; Pasquarè et al., 1992) following the methodology proposed for recent geological maps of volcanic areas (e.g. Bonomo and Ricci, 2010; Branca et al., 2011; Lucchi, 2013; García Sánchez et al., 2019). Lithosomes are informal stratigraphic units designating a stratigraphically and morphologically recognizable volcanic center (Wheeler and Mallory, 1953). Applying this methodology, we can use objective and field data to define the lithostratigraphic units directly on the field and, at the same time, we can show the spatial distribution of the main lava domes defining lithosomes.

More than 100 samples have been collected in the field identifying descriptive textural markers (Table 1) for the hand specimen and thin section scale textural analyses. Back-scattered electron imaging analyses were also performed using AMRAY 1830 instruments with EDAX PV9800 spectrometer at 20 kV at the Dept. of Petrology and Geochemistry, Eötvös Loránd University, Hungary. Lithofacies classification of silicic dome architecture is based on previous classifications improved in different volcanic environments (subaerial: Duffield et al., 1995; Stevenson et al., 1994a, b; Lexa et al., 2014; subglacial: Tuffen and Castro, 2009; submarine: Németh et al., 2008).

Radiometric geochronology, using the Cassignol-Gillot K/Ar dating method, was carried out in ATOMKI Institute for Nuclear Research of the Hungarian Academy of Sciences in order to refine the timeframe volcanism of TLDF. During samples separation special attention has been payed to remove xenocrysts and weathering crust of the collected samples. The fresh samples was first mildly crushed and sieved and the 0.125–0.25 mm size fraction was selected for further treatment. Volcanic glass was separated by heavy liquids with density ranges of typically 2,6–2,65 g/cm^{-3}. The separate was ultrasonically washed in deionized water.

The potassium content was measured on 50 mg sample aliquots after dissolution by HF and HNO_3, by a Sherwood-400 type flame spectro-photometer with an accuracy better than ±1.5%. Ar was measured by a low-background MAP-215-50 noble gas mass spectrometer. Whole-rock samples were heated at 100 °C for 24 h under vacuum to remove atmospheric Ar contamination that adsorbed on the surface of the mineral particles during sample preparation. Argon was extracted from the minerals by fusing the samples by a resistance heating furnace at 1800 °C. The released gases were cleaned in two steps in a low-blank vacuum system by Zr-Al and Ti-getters.

To date the selected samples the Cassignol-Gillot K/Ar dating technique was used. Details and advantages of this method were discussed by Cassignol and Gillot (1982), Gillot and Cornette (1986). Low Ar background, high signal to noise ratio, and the stability of the ion source parameters of the mass spectrometer allowed the application of the non-spike K/Ar dating method. The accuracy and reproducibility of the isotope ratio measurements were periodically controlled by the HDB-1, GL-O and BB-6 international standards. The decay constants recommended by Steiger and Jager (1977), were used for age calculation with an overall error of ±2%.

4. Results

4.1. Stratigraphy of the Telkibánya lava dome field

The TLDF volcanic complex covers an area >25 km^2 and represents the western segment of the silicic volcaniclastic and lava dominated area (Fig. 2). The succession has been divided into stratigraphic units based on their lithology, composition, geochronology and stratigraphic position. The oldest outcropping succession (Kiss and Zelenke, 2009; Molnár et al., 2009) is made of hydrothermally altered lava flows and intrusive rocks, resulted from the construction of an edifice building andesitic volcanism (Kánya Hill andesite Figs. 3, 12.4 ± 0.5 Ma - Pécskay et al., 1987; Molnár et al., 2009). Their erosional remnants are exposed in an uplifted position north

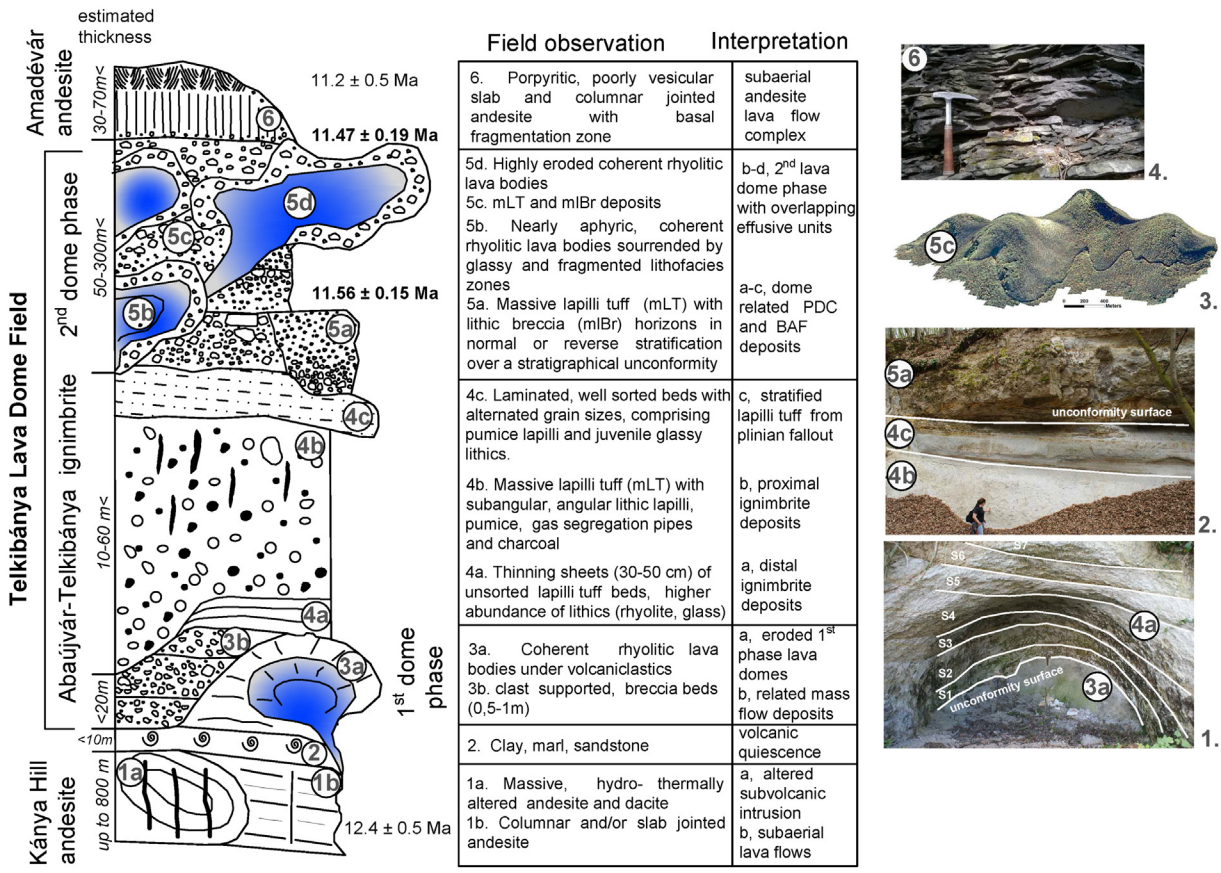

Fig. 3. Stratigraphic succession recognized in the investigated area (vertical range not in scale). Radiometric age references are in Table 2. Pictures illustrating the stratigraphy: 1. Stratigraphical unconformity between eroded body of the 1st lava dome phase (3a) and distal sheets of Abaújvár-Telkibánya Ignimbrite (4a). 2. massive lapilli tuff (4b) and stratified lapilli tuffs (4c) units of Abaújvár-Telkibánya Ignimbrite. The lithic breccia units at the top of the picture represents the initial block and ash flow deposit of 2nd phase Telkibánya lava domes. 3. Morphology of the eroded 2nd phase lava domes using SRTM digital elevation modell and Google Earth imaging 4. slab jointed andesite (6).

of the TLDF (Fig. 2) and partially covered by shallow marine sediments (Fig. 3). Marine sediments are usually of reduced thickness (<10 m), poorly exposed and thickened easternward (100 m, Ilkey-Perlaki, 1978). The foraminifera population (e.g. *Elphidium crispum*, Rotalia beccari) is suitable for biostratigraphy studies, indicating a shallow marine sedimentation (Late Badenian - Early Sarmatian NN5, NN6 biozone, Szentgyörgyi, 1978; Kováč et al., 2007, 2018) and testifying an important volcanic break in the succession.

The following TLDF succession comprises mostly unaltered silicic lavas that can be divided into lower and upper lava dominated units (respectively 5b and 5d of Fig. 3) separated by different volcaniclastic lithofacies associations. The whole TLDF deposits are high-silica (SiO_2: 74–77%), crystal-poor (≤5% modal phenocrysts) vitrophyric rhyolites, containing dominantly plagioclase and sanidine, subordinately quartz and biotite, and rarely amphibole (Szepesi, 2009).

The TLDF succession started with coherent remnants of glassy (coherent perlite) rhyolitic lavas (Fig. 3, n. 3), defined as the 1st lava dome phase. The rare outcrops are exposed in the western part of the lava dome field. Subordinate monolithologic pumiceous breccia sheets are also identified (Fig. 3, n. 3b). The 1st phase lava dome thickness is only estimated up to tens of meters because of the lack of base exposure. The absence of hyaloclastite type fragmentation promotes the assumption of a regression event before the onset of the dome building volcanism. The dominance of coherent lithofacies associations indicates erosion of fragmental autoclastic parts of dome edifices.

The overlying Abaújvár-Telkibánya ignimbrite succession is identified as a stratigraphic marker horizon that separates the TLDF lower (1st phase, n. 3 in Fig. 3) and upper (2nd phase, n. 5 in Fig. 3) lava dome units. The ignimbrite thickens in north-western direction and vertically comprises three major units (Fig. 3, n. 4). The lower, non-welded massive lapilli tuffs (mLT < 30 m) contain charcoal and gas segregation pipes (Fig. 3 n. 4a) usually overlain by stratified, well sorted pumice fall deposits (sLT, 1–5 m). The identified Miocene gullies indicate an erosional gap after volcaniclastic deposition.

The subsequent extrusions of silicic lavas (2nd phase) and dome related volcaniclastic deposits form a complex succession of rhyolitic flow/dome lithosomes (Fig. 3, n. 5). Spatial distribution of the TLDF bodies (Fig. 4) follows the regional Late Miocene extensional stress field (Fodor et al., 1999; Petrik et al., 2014) with NW-SE (and perpendicular) striking fault systems, which is highlighted by the current valley directions (Ósva, Sényő valleys). The slopes are usually covered by rhyolite debris of higher altitude coherent bodies (Fig. 4), but some exploration boreholes (Ilkey-Perlaki, 1967, 1972, 1978; Gyarmati, 1981) revealed detailed vertical lithofacies architecture and sometimes give information about the horizontal changes. The lavas have an intrusive contact (host rock is the ignimbrite) or overlie the erosional surface. The clast-supported, monolithologic breccias (<10 m) and unsorted layers of lithic rich lapilli tuffs have been identified as dome related block and ash-flow (BAF) and pyroclastic density current (PDC) deposits filling erosional gullies. The recurrent vertical alternations of the coherent and autoclastic lithologies in the borehole sequences indicate overlapping bodies (Figs. 3, 4, 5 2a and b phase) in the succession. The topmost occurrence of the lavas was drilled at 550 m a.s.l. (Tb6 Bh. Fig. 5). The present erosion level (250–300 m a.s.l) and the deep-

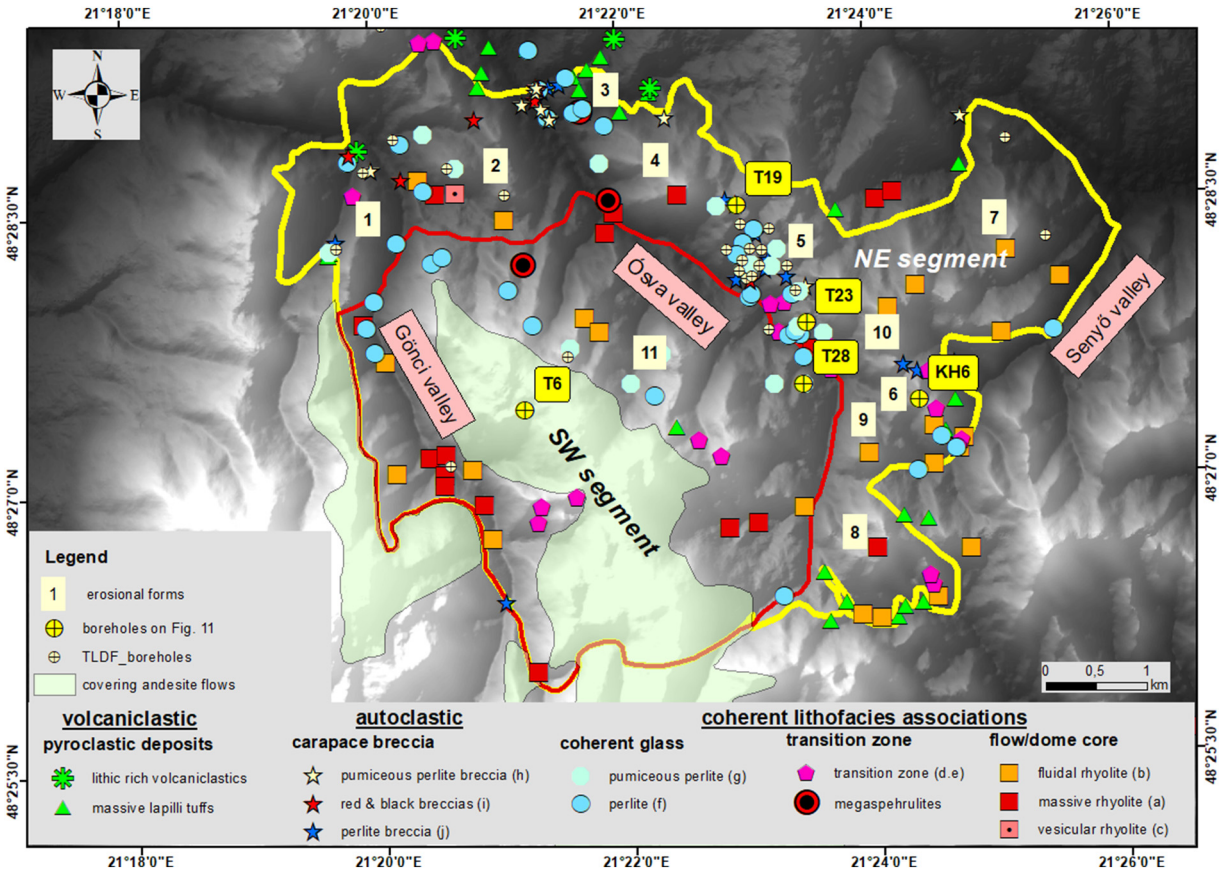

Fig. 4. Lithofacies cropping out in the Telkibánya Lava Dome Field. Yellow circles refer to the boreholes displayed in Fig. 5. Numbers refer to location of remnants of dome morphology after 10 Ma erosion described in Tables 3a,3b: 1. Varga Hill, 2. Kerek-Vas Hills, 3.Templomdomb, 4. Cser Hill (Fig. 13c), 5. Kőgát Hill, 6. Csoszota Hill, 7. Ó-Gönc Hill, 8. Solymos Hill, 9. Tér Hill, 10. 2nd phase top peaks (Fig. 13b), 11. andesite covering the SW block (Fig. 13a). Digital elevation map: SRTM Data. (For interpretation of the references to colour in this figure legend, the reader is referred to the web version of this article.)

est boreholes (Fig. 5) reached only coherent lithofacies associations, so the total thickness of the successions is over 300 m.

We dated the lower (2a phase) and upper (2b phase) part of TLDF lava succession (Fig. 2), which give overlapping ages of 11.56 ± 0.15 Ma and 11.47 ± 0.19 Ma, respectively (Fig. 3). These new unspiked Cassinol-Gillot ages give reduced uncertainties compared with the conventional K/Ar method (Table 2) and better constrain the age of activity.

Andesitic to dacitic effusive volcanism (Amadévár andesite) ended the Miocene eruptive succession and its products partly cover the western part of TLDF area (Amadévár andesite, 11.2 ± 0.5 Ma, Pécskay et al., 1987, Figs. 2 and 3).

This new stratigraphical framework, constrained by radiometric data, indicates that TLDF comprises the latest high silica lava effusive event in the region, followed by andesitic calc-alkaline volcanism.

4.2. Lithofacies architecture of the silicic lava domes and flows

The combination of stratigraphic and petrographic analyses results in the identification of 12 lithofacies of coherent and autoclastic lithofacies (sensu McPhie et al., 1993) (Tables 2, 3a, and 3b). These lithofacies has subsequently been organized in 6 facies associations for the definition of the flow/dome architecture, according to Manley and Fink (1987), McPhie et al. (1993), Stevenson et al. (1994a).

5. Discussion

5.1. The Telkibánya Lava Dome Field lithofacies architecture in comparison with other examples

Effusive silicic volcanism produces extreme textural heterogeneity within flows and domes from their inner coherent core to the autoclastic carapace (Calder et al., 2015). The field and subsurface investigation of obsidian flows established a layered structural model (Fink, 1983; Manley and Fink, 1987; Fink et al., 1992; Stevenson et al., 1994a; Denton et al., 2012; Shields et al., 2016). Therefore, the bodies of TLDF exhibit textural zonation (Fig. 11) alike to those shown by some examples of Holocene rhyolite flows (Little Glass Mountain, Fink, 1983; Obsidian Dome, Manley and Fink, 1987; Ben Lomond, New Zealand, Stevenson et al., 1994a). The lithofacies architecture comprises coherent (Table 3a) and autoclastic (Table 3b) lithofacies representing distinct parts (proximal, medial and distal) of the edifices where devitrified zones occur in proximal area grading outward into glass bearing lithofacies associations. The dense, crystalline, non-vesicular textures of the massive (*zone a*, Fig. 11b) and flow banded type (*zone b*, Fig. 11c) microcrystalline rhyolite facies, indicate slowly cooling melt that accumulated around the vent or spread gravitationally as a viscous body, respectively (Duffield et al., 1995). The subordinate, locally occurred vesiculated microcrystalline lithofacies (Fig. 11b) reflects uneven volatile distribution within flow, where the vesiculation is mainly secondary, caused by crystallization of lava interior (Tuffen and Castro, 2009).

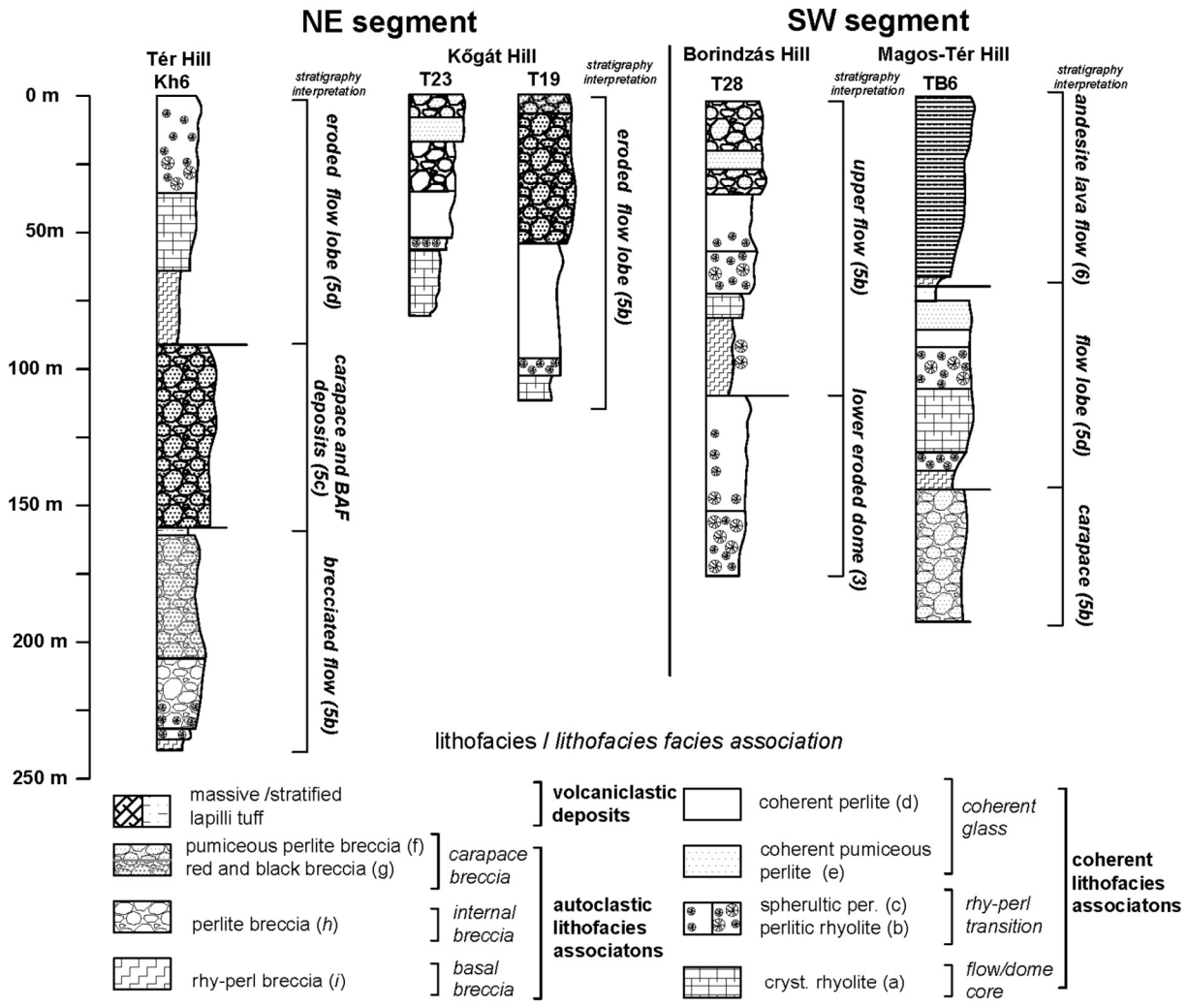

Fig. 5. Borehole stratigraphy of Telkibánya Lava Dome Field. For location of the boreholes, see Fig. 4c Data from Ilkey-Perlaki (1967, 1972), Gyarmati (1981).

The spherulitic textural transition between the microcrystalline rhyolite and coherent glassy zones has been identified in most obsidian flows (Manley and Fink, 1987; Richnow, 1999; Bullock et al., 2018) and is separated as an individual structural layer in the flow stratigraphy of Ben Lomond rhyolite lava flow (Stevenson et al., 1994a). The cooling rate differences relative to glass transition can be reflected in the ratio of microcrystalline and glassy parts identifying perlitic rhyolite (*zone d*) and spherulitic perlite (*zone e*) lithofacies zones (Fig. 11b, c). The unique "megaspherulites" (*zone d*, Fig. 11b) reported from rare occurrences (Simon, 1962; Smith et al., 2001; Polo et al., 2018) can provide a special record of the thermal history of host lava (Befus et al., 2014).

The dense coherent perlite zone (*zone f*) with moderate to low porosity (5–20%) is similar to the (upper) obsidian layer of studied Holocene flows (OBS, Manley and Fink, 1987; Richnow, 1999). However, in the TLDF all glass facies hydrated (up to 5% H_2O, Ilkey-Perlaki and Szöőr, 1973; Szepesi, 2009) to form perlite. Moving outwards, decreasing lithostatic load enabled melt vesiculation (Fink and Manley, 1987) creating pumiceous groundmass. The high porosity values (6–30%) and textural characteristics of the pumiceous perlite (*zone g*) match with the "finely vesicular pumice" lithofacies described from young examples (FVP, Fink, 1983; Fink and Manley, 1987; Stevenson et al., 1994a, b; Richnow, 1999).

The fragmented lithofacies associations (Table 3b) developed by autoclastic fragmentation of the flow crust (Fink and Manley, 1987; McPhie et al., 1993), which breaks into fragments with variable grain-sizes (mm-m). The pumiceous perlite breccia (*zone h*) is a quenched autobreccia (Fink, 1983) of the pumiceous perlite (*zone g*) with generally high porosity. The red and black breccias (*zone i*) have not been interpreted from the CPR region before. The

Table 2
K-Ar radiometric ages of the Telkibánya Lava Dome Field (w.r.: whole rock) performed using the Cassignol-Gillot method.

Lithology	Coordinates		Sample	Material dated	K%	40Ar* [cm3/g]	40Ar* [%]	Age (Ma)	±1σ	Ref.
	Lat	Long								
Perlitic rhy.	48.4775	21.3385	Nagy Farkas Hill (2b phase)	w.r.	4.036	$1820*10^{-6}$	21	11.47	0.19	This study
Perlite	48.4645	21.3511	Kerek Hill (2a phase)	w.r	1.891	$8460*10^{-7}$	13	11.56	0.15	This study
Perlitc rhy.			Susulya	w.r	3.48	$1.527*10^{-6}$	21	11.2	0.7	Pécskay et al., 1987
Rhyolite			Cser Hill	w.r	3.62	$1.662*10^{-6}$	84.2	11.7	0.5	Pécskay et al., 1987
Andesite			Fehér Hill	w.r.	1.65	$0,802*10^{-6}$	28	12.4	0.7	Pécskay and Molnár, 2002

Table 3a
Description and interpretation of coherent lithofacies associations in the Telkibánya Lava Dome Field. Location of key outcrops in Fig. 4.

	Facies associations	Lithofacies zones	Distribution and thickness (*localities*)	Description	Interpretation	References
Coherent part of the lava dome/flow edifices	Micro-crystalline core	Massive (zone a)	Thick (30–100 m), irregular shaped part of steep sided (coulee, dome) erosional forms(*2,4, 5, 8, 10*)	Red to pink coloured, weekly to non-vesicular microcrystalline groundmass (poikilitic, felsitic,) with subvertical foliation and jointing (Fig. 6a.), spherulite up to cm, rare litophysae.	Proximal regions of dome edifices close to supposed vents, prolonged groundmass crystallization above glass transition.	Bonnichsen and Kauffmann, 1987; Duffield et al., 1995; Richnow, 1999; Orth and McPhie, 2003
		Banded (zone b)	Stretched layers (10–25 m) with larger areal extent and variable thickness (*2–11*)	Light brown to grey coloured, banded (mm to cm), micro- to crypto-crystalline groundmass with strong planar alignment. Sub-horizontal fracture set (cm to dm thick, Fig. 5b). Meso or micro scale folding. (Fig. 6c) Spherulites in several generations (mm to cm), abundant lythophysae	Proximal facies of spreading flow lobes with jointing parallel to the bedrock. The foliated texture indicates internal ductile strain. Folding occurs in flow compressional zones.	Bonnichsen and Kauffmann, 1987; Cas and Wright, 1987; Duffield et al., 1995
		Vesicular (zone c)	Rare outcrops with boulders forming irregularly shaped and thickened zones (1–5 m)(*2–5, 11*)	Light brown to pink coloured, highly vesiculated (up to 40%, Fig. 6d.) microcrystalline groundmass with variable vesicle size (mm to cm) and shape (equidimensional, elongated, coalesced).	Proximal facies of dome and flows with unequal volatile distribution. Groundmass crystallization induced vesiculation. The internal strain caused elongation and distortion of vesicles.	Stevenson et al., 1994a, b,Manley and Fink, 1987Tuffen and Castro, 2009
	Transition belt	Perlitic rhyolite (zone d)	Irregular thickness (up to 40 m) and geometry (horizontal or vertical) coupled with zone e*1,2,4–11*	Alternation of the predominant brown to pink microcrystalline and darker glassy groundmass. Low angled, gradual foliated (mm to dm) transition (Fig. 7a) from perlite to flow banded rhyolite (zone b), outcrop scale folding and slab jointing (Fig. 7b). Large, curvy, radially jointed spherulites (10 to 50 cm) in the perlite adjacent to the massive rhyolite (Fig. 7c, d). Smaller, blister-shaped spherulites around the larger ones. Brown spherulitic bands (mm to cm) contains magnetite microlites (Fig. 7e) in a vesicular glassy matrix. Weak perlitic fracturing of the glass, lithophysae abundance in microcrystalline bands.	Groundmass crystallization dominate part of transition belt with subordinate hydration and perlitic fracturing in the glasstwo different type of transition:1. Banded transition in flow lobes;2. megaspherulitic transition around the massive rhyolites (vent regions).Volatile oversaturation for lithopysae development.	Silver Cliff, Colorado Smith et al., 2001; Klondyke, Arizona Simon, 1962; Parana Magmatic Province Polo et al., 2018; McPhie et al., 1993; Breitkreuz, 2013
		Spherulitic perlite (zone e)	Irregular thickness (up to 40 m) and geometry (horizontal or vertical) coupled with zone d*1,2,4–11*	Alike to zone d with dominant glassy groundmass. A 2 m-wide dyke-like structure (Fig. 7f) widening (5 m) upward. Subvertical foliation perpendicular to the dyke walls. Lithophysae (cm to dm) in the microcrystalline bands.	Glass and hydration dominated part of the transition.A feeder dyke occurrence at the dome base (Cser Hill).	Inyo domes (Fink, 1985), Douglas Knob, USA (Befus et al., 2014) Hrafntinnuhryggur, Iceland (Tuffen and Castro, 2009).
	Coherent glass	Perlite (zone f)	Mainly cropping out in areas at low altitude (below 400 m a.s.l.), variable thickness (3–50 m), sporadic occurrences exposed under the volcaniclastite series (Fig. 3), (*1–6, 8,9,11*).	Dark grey massive or banded (mm to cm) texture with sub-horizontal or subvertical orientation. Dense perlitic fracturing defined at macro (dm wide globular jointing Fig. 8a) and micro scale (Fig. 8c). Perlitic bead diameters from 100 to 250 μm, bounded by curved longitudinal cracks (0,5-1 mm Fig. 8c) Irregular subvertical shrinkage surfaces (Fig. 8a). Local 0,5 to 1 m spaced columnar jointing. Rare basal perlite (m) under microcrystalline rhyolite (boreholes Fig. 5).	Medial, sections of silicic lava domes and flows. The dense, glassy texture indicate larger flow depth (30–50 m)Intensive syn and post volcanic hydration	Bonnichsen and Kauffmann, 1987; Manley and Fink, 1987; Richnow, 1999; Anovitz et al., 2008; Németh et al., 2008; Denton et al., 2012; McPhie et al., 1993
		Pumiceous perlite (zone g)	Poorly exposed part with variable thickness (1–40 m) around coherent part edifices mainly in lower altitude regions(*1–6, 9, 11*)	Light grey, vesicular glassy groundmass with subvertical or subhorizontal (Fig. 8b.) foliation. General transition to coherent (zone e) and autoclastic part (zone f and g). Upward increasing.in porosity from 5% to 50%, Well-developed foliation with bands of different vesicularity, shearing and coalescence (Fig. 8d). Magnetite microlites preferentially on vesicle rims (Fig. 8c, d). Subordinate perlitic fracturing.	The external part of the flows/dome coalescence and stretching were induced by local strain differences in the flow. Magnetite crystallization on the solidified vesicle walls occurred during cooling.	Fink, 1983; Stevenson et al., 1994a, b; Fink and Manley, 1987; Richnow, 1999; Tuffen and Castro, 2009; Tuffen and Castro, 2009

Table 3b
Description and interpretation of autoclastic lithofacies associations in the Telkibánya Lava Dome Field. Location of key outcrops in Fig. 4.

	Facies associations	Lithofacies zones	Distribution and thickness (*localities*)	Lithology	Interpretation	References
Autoclastic part of dome/flow edifices	Outer (carapace breccia)	Pumiceous perlite breccia (zone h)	Exposed in deep gullies at margin of TLDF and drilled in variable thickness (10–50 m),*1–6,9,11*.	Matrix poor (20%), clast supported, monomictic breccia (Fig. 9a), Clast rotation observed in the fragmental -coherent transition (Fig. 9a). Internal fragmented layers (5-25 m) inside coherent parts also developed. Clasts: sub-angular to subrounded (cm to <0.5 m from zone f) matrix: massive fine angular pumiceous shards (0.1–1 mm) and crystal fragments (Fig. 8c), occasionally oxidized and/or slightly argillified.	Quench fragmented autoclastic carapace (down to 50 m in depth) around the inner coherent lava core (Fig. 10a, c), clay alteration of the matrix caused by subsequent weathering under subtropical Miocene climate.	Anderson et al., 1998; Bonnichsen and Kauffmann, 1987; Duffield et al., 1995; Richnow, 1999; Maeno and Taniguchi, 2006
		Red & black breccia (zone i)	Elongated lens (20–100 m) or fissure-like geometry in zone e and f with variable thickness(3–70 m) (*2,3,5,9*)	Clast (cm-dm) supported breccia with reddish oxidized matrix, and clast alignment texture (Fig. 9b, d). Clasts: subangular to subrounded perlite (mm to dm, zone f, Fig. 9d). Matrix: red coloured vesicular glass fragments (0.1–1 mm). Radial fracturing filled with vesicular reddish matrix in the perlitic clasts. Clast alignment and annealing of shards.	Controversial interpretation in the literaturea, development of compressional and extensional regime with flow folding with shear induced fragmentation and oxidationb, more likely explosive fragmentation formed explosion pits (fissures) on the lava surface as a result of local vapour overpressure (final welding with compaction, clast alignment).	Manley, 1996, Maeno and Taniguchi, 2006; Fink and Manley, 1987; Stevenson et al., 1994a; Calder et al., 2015
	Internal (subordinate)	Perlite breccia (zone j)	Lense-like (m) or irregular zones in the coherent perlite, thickened layers (m to 10 m) between zone e and f (1,*3,5*)	Clast supported, monolithic breccias with white coloured matrix, jigsaw fractured clasts or clast rotated arrangement (Fig. 10a), increasing clast size toward the fragmental-coherent transition. Clasts: angular-subangular perlite (mm-dm, zone f). Matrix: white-pale yellowish coloured, angular glass shards (<mm) <20 vol%	Autoclastic breccia of the coherent perlite.Deformation of the outer carapace caused local shear stress concentration and fragmentation in the coherent zone.	Richnow, 1999;Tuffen and Castro, 2009.
		Rhyolite breccia (zone k)	Local exposures (<m) or drilled in boreholes (3–25 m)*5*	Brown to pink, clast supported monolithic breccias (Fig. 10b.) with microcrystalline groundmass, restricted clast alignment and flattening. Clast: subangular rhyolite clasts (mm to dm). Matrix: microcrystalline rhyolite and crystal fragments (<mm)	Shear induced autoclastic fragmentation in internal rhyolitic coherent zones during the solidification by possible blocking of the flow movement.	Richnow, 1999;Fink and Manley, 1987.
	Basal (subrodinate)	Rhyolite -perlite breccia (zone l)	variable thickness (3–26 m)*1,5*	Brown to pink heterolithologic breccia with jigsaw fractures, clast alignment, and minor clast flattening. Clasts: angular to subrounded microcrystalline rhyolite and dense glass (perlite). Matrix: massive pinkish coloured (<mm). Weathering observed (Kőgát Hill).	Autoclastic fragmentation in the basal shear zone of the silicic flows. The large thickness indicates overriding talus apron.	Ngongotaha dome, New Zealand (Richnow, 1999); Snake River Plain, USA (Bonnichsen and Kauffmann, 1987). Other examples in Bull and McPhie (2007); Smith (1996); Sweetkind and Bova (2015).

locally observed red and black breccias underlie or break through this pumiceous material. The textural differences between them suggest alternative fragmentation process for the red and black breccias and their textural characteristics are very similar to explosion breccias of obsidian flows (Bonnichsen and Kauffmann, 1987; Castro et al., 2002; Fink and Manley, 1987; Manley, 1996; Richnow, 1999; Stevenson et al., 1994a, b).

Internal breccias (*zone j and k*) containing dominantly coherent clasts suggest that they developed by internal shear stress during extrusion movements (Richnow, 1999). Fracturing in the dense glass (*zone j*) could be associated with the deformation of the outer carapace (Tuffen and Castro, 2009). Development of internal fragmental zones with microcrystalline groundmass (*zone k*, Fig. 11c) is also common in silicic lava flows (Manley and Fink, 1987; Richnow, 1999) suggesting deep rooted fractures. Large fragmentation depth through the whole transition zone and reaching the crystalline rhyolite core could be explained by large scale blocking of the flow in distal position.

The "coarsely vesicular pumice" (CVP) unit defined in North-American rhyolite flows (Fink and Manley, 1987) with very low density (down to 0.8 g/cm^3, Fink, 1983) was not observed in TLDF. This layer is also missing from the Okataina Volcanic Centre rhyolite flows (New Zealand), which implies that CVP is absent as a continuous layer from thick, high silica rhyolite lavas (Stevenson et al., 1994a, b; Richnow, 1999) and probably restricted to smaller silicic bodies.

Table 4
Identification of the major lithostratigraphic units, individual lithologies and structural features in Telkibánya Lava Dome Field. The morphological units are gathered into lithosomes referring to primary volcanic edifices. Abbreviations: mLT: massive lapilli tuff, sLT: stratified lapilli tuff, mlBR: massive lithic breccia.

		Morphological unit	1. Varga Hill	2. Kerek Hill	3. Temlomdomb	4. Cser Hill	5. Kőgát	6. Tér Hill	7. Csoszota	8. Solymos	9. Ó-Gönc	10. Small rhyolite peaks	11. Andesite covered SW block
		Lithosome	Kerek Hill Flow		Cser Hill Coulée		Kőgát flow		Csoszota dome	Solymos dome		2 phase flow remnants	
		Top elevation and (base), m a.s.l	422 (240)	416 (240)	290 (240)	505 (240)	420 (300)	503 (325)	478 (210)	546 (425)	513 (370)	522 (400)	720 (250)
Telkibánya Lava Dome Field	Lithostratigraphic units	1st dome phase	Not id.	X	X	X	Not id	X	X	Not id.	Not id.	Not id.	X
		Abaújvár-Telkibánya volcaniclastics	mLT, sLT, mlBR	mLT, sLT, mlBR	mLT, sLT, mlBR	mLT, mlBr	mLT	mLT, mlBR	mLT, mlBr	mLT	Not id.	Not id.	mLT
		2nd dome phase	2a	2a	2a	2a,2b	2a	2a,2b	2a,2b	2a,2b	2b	2b	2a, 2b
	lithofacies zonationand structural elements	Pumiceous Perlite breccia	X	X	X	X	X	X	X	Not id.	Not id.	Not id.	Subordinate
		Red & black breccias	Not id.	X	X	Not id.	X	X	Not id.	Not id.	Not id.	Not id.	Not id.
		Internal breccia	X	Not id.	Not id.	Not id.	X	Not id.	Not id.	Not id.	Not id.	Not id.	Not id.
		Basal breccia	Not id.	Not id.	Not id.	Not id.	X	X	Not id.	Not id.	Not id.	Not id.	X
		Pumicous perl.	X	X	X	X	X	X	X	Not id.	n.i	Not id.	X
		Coherent perlite	X	X	X	X	X	X	X	X	Not id.	Not id.	X
		Transition zone	X	X	X	X, feeder	X	X	Not id.	X	X	X	X
		Megaspherulites	Not id.	Not id.	X	X	Not id.	Not id.	Not id.	Not id.	Not id.	Not id.	X
		Massive rhyolite	Not id.	X	Not id.	X	X	Not id.	Not id.	X	Not id.	Not id.	X
		Fluidal rhyolite	Not id.	X	X	X	X	X	X	X	X	X	X
		Vesicular rhy.	Not id.	Not id.	X	X	X	Not id.	Not id.	Not id.	Not id.	Not id.	X
		Folding	Not id.	Not id.	not id.	Not id.	Not id.	X	Not id.	Not id.	Not id.	Not id.	Not id.
		Jointing	Not id.	X (v)	X (v)	X (v)	X (v, h)	X (h)	Not id.	Not id.	Not id.	X (h)	X (v, h)

Fig. 6. Textural characteristics of coherent microcrystalline rhyolite lithofacies associations (zone a, b, c) a) Subvertical jointing in the core region (zone a) of Kőgát flow suggesting proximal, close to vent, position. b) Closely spaced sheeting joints of the rhyolite (zone b) dipping in the flow direction from Tér Hill. c) Foliated fabric of the flow banded lithofacies zone showing hand specimen scale folding of Ork Hill (zone b). d) Vesicular microcrystalline lithofacies (zone c) at the base region of Cser Hill coulee (scale = 4 cm).

5.2. Distribution of the lithofacies in the Telkibánya Lava Dome Field

The horizontal correlation of the lithofacies architecture (Fig. 4), the textural-structural characteristics and the lithofacies geometry clearly define the proximal, medial-distal flow segments (Fig. 12) and their inherence. At least 5 separable lithosomes (i.e. flows, coulees and domes) can be identified in the area which were erupted during the 2a phase (Table 4, Fig. 12). The frontal and upper carapace zones of the 1st and 2b phase (except below andesite, Fig. 13a) flows/domes are nearly entirely eroded. Summarising the current morphology and flow stratigraphy the Kerek Hill and Kőgát Hill are the two largest flow remnants (<1 km^2, Fig. 12). Their length to height ratio (ca. 10:1) suggest larger volume of spreading lobes at the expense of melt accumulation above vents (Sweetkind and Bova, 2015). The related exposed massive rhyolite lithofacies with subvertical jointing reveal the possible vent regions of both units (Fig. 12). The medial-distal flow lobe of Kőgát Hill can be traced 2 km long in the borehole profiles (T23 and T19, Fig. 5). Here, the pumiceous carapace opened up by explosion pits as proved by the presence of the red and black breccias in several points (Figs. 4, 12).

Erosion reached the coheNrent perlite lithofacies depth, but the microcrystalline core of the flow lobes was only exposed by few drillings. Small erosional hills (Fig. 13b) emerge above the usual surface of Kőgát Flow, where the low angled foliation (Kh6, Fig. 14a) indicates that these represent the coherent core of a quite large flow structure. The morphology of 2b phase flow remnants suggests multi-lobe emplacement of the silicic effusions (Fig. 12). The subsurface dataset under the andesite flows (SW block) with reduced lava thickness (65 m) submits its distal position which is in good agreement with published lobe heights at frontal flow ends (Fink, 1983; Sweetkind and Bova, 2015).

Dome-shaped (1 km^2) erosional cones are located at the margins of TLDF (Cser Hill Fig. 13c, Csoszota, Solymos). Their relative elevation (ca 350 m) with low area to height ratio (5:1) indicate melt accumulation zones above vents (Duffield et al., 1995; Sweetkind and Bova, 2015).

The current surface ratio of the coherent and autoclastic (2.5 km^2) lithofacies associations is 10:1, but boreholes revealed higher subsurface proportion of the autoclastic material (up to 1:1, Fig. 5). Comparing dimensions of the TLDF lavas with recent subaerial silicic edifices is only possible in case of the least eroded 2a phase. The original thickness of these bodies is estimated between 100 and 200 m with a ca 3 km spreading length, according to the traceable subsurface occurrences of Kőgát and Kerek Hill flows (Fig. 12). The 12.9 Ma lava flows of the Calico Hills Formation (Sweetkind and Bova, 2015) present similar size (120–240 m thickness with 3–5 km length). The other well-known subaerial examples are smaller, and the flow layering is different. The Little Glass Mountains (California, USA, Fink, 1983) has 120 m thickness and 2 km length but its characteristic coarsely vesicular pumice layer is absent from TLDF. The Rocce Rosse flow (Lipari, Italy) is a 100 m thick, 2 km long aphyric obsidian flow where the extreme textural heterogeneity come from an inferred complex emplacement history (extensional strain, progressive and brittle deformation, Bullock et al., 2018) coupled with other degassing and hydration processes (Shields et al., 2016)

5.3. Emplacement model and evolution of the Telkibánya Lava Dome Field

Lava flows and domNes are emplaced in various volcanic settings (subaerial, submarine, subglacial, cryptodomes) and produce wide range of textures including coherent and autoclastic lithologies. The textural characteristics of the autoclastic part are controlled by the emplacement conditions (McPhie et al., 1993). The strong interaction between lava and water cause pervasive hyaloclastite type fragmentation in submarine (Ponza, Italy - De

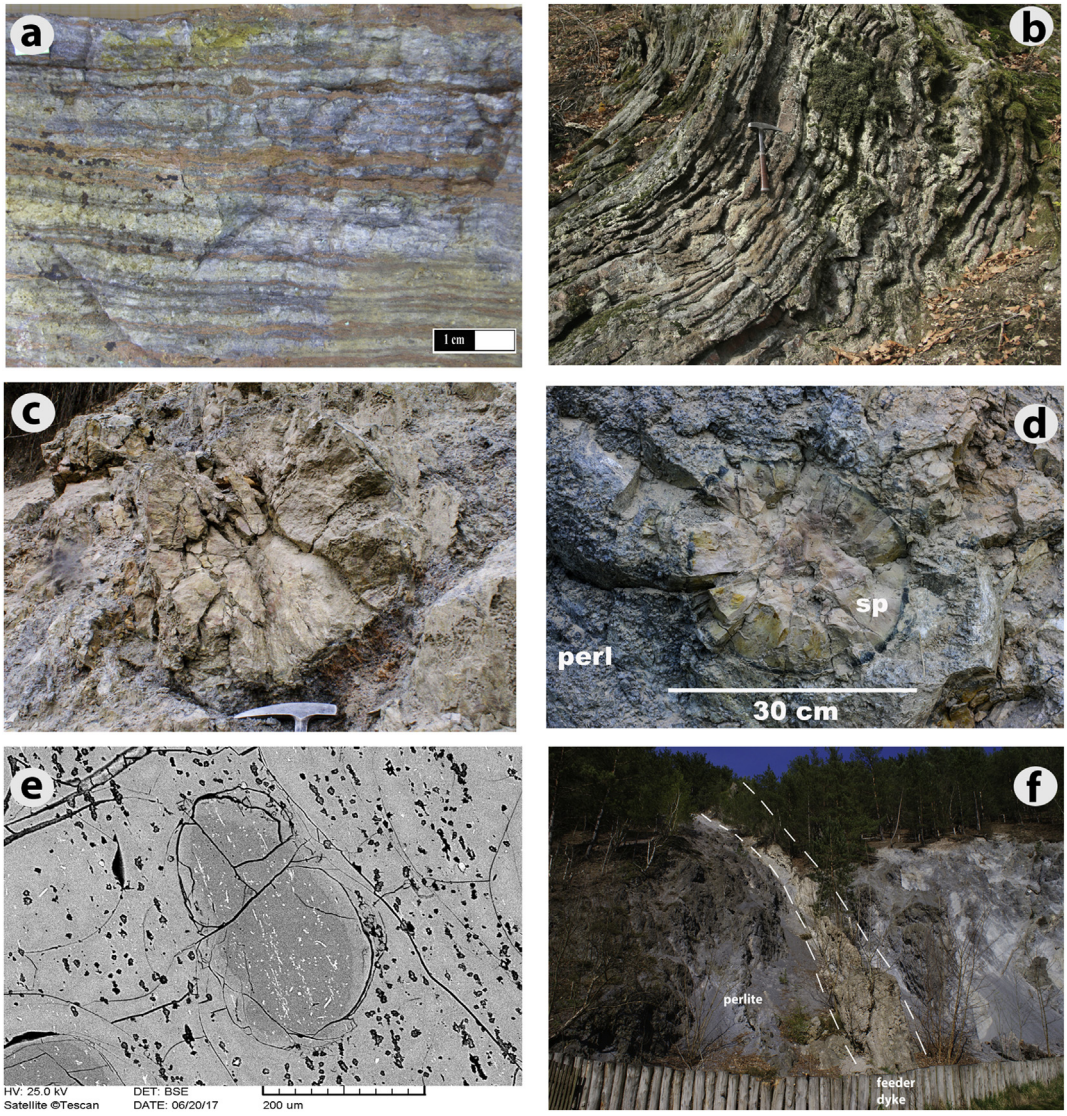

Fig. 7. Textural characteristics of rhyolite-perlite transition lithofacies association (zone d, e). a) Banded appearance of the rhyolite-perlite transition with red coloured rhyolitic and grey perlite bands (zone d). b) Limb of a flow fold composed of slab jointed perlitic rhyolite lithofacies (zone d) at Tér Hill c) The largest "megaspherulite" (<0.5 m) found in perlite from the perlite–rhyolite transition zone (zone e) at the base of Cser Hill. d) "Megaspherulite" in perlite (zone e) with well-defined radial structure and dark black outer boundary layer. e) Backscattered image of spherulitic perlite lithofacies (zone e). The dark spherulites show higher abundance of magnetite microlites, while the surrounding glass is highly microvesicular. f) 15 m high spherulitic perlite (zone e) cliff in the coherent perlite (zone f) at base of Cser Hill, which is interpreted as being a basal part of a feeder dyke cutting through the perlite zone. (For interpretation of the references to colour in this figure legend, the reader is referred to the web version of this article.)

Rita et al., 2001; Pálháza - Németh et al., 2008; Cabo de Gata, Spain - Porreca et al., 2014) and subglacial environments (Hrafntinnuhryggur, Iceland - Tuffen and Castro, 2009). In the TLDF area, a series of silicic effusive eruptions were deposited mainly in a subaerial environment. The older volcanological interpretations (Ilkey-Perlaki, 1972, Csillag and Zelenka, 1999) refer to a submarine emplacement model for this effusive silicic volcanism and the perlite formation, without mentioning the subaerial flows and domes.

Considering the results of this work, a 3-stage evolutionary model is proposed for the TLDF emplacement and evolution, as depicted in Fig. 14. Stage 1 involves effusion of the 1st lava dome phase (Fig. 14a). The results of research drillings and geological mapping (Ilkey-Perlaki, 1967, 1972; Gyarmati, 1981) allow the identification of a sedimentary formation as bedrock (Fig. 3). The subsequent autoclastic textural variations of the lava without hyaloclastite type fragmentation could not support the presence of marine conditions. Thus, the 1st dome phase emplaced after a regression event in subaerial environment (Fig. 14a), and the dominant coherent lithofacies associations and sporadic breccias indicate remarkable erosion before the onset of the subsequent volcaniclastic sedimentation (Stage 2).

Stage 2 involves the formation of Abaújvár-Telkibánya ignimbrite (Fig. 14b) with a 3-part lithofacies architecture (Fig. 3) The observed thickness of the massive and stratified lapilli tuffs, the associated depositional features (gas segregation pipes, charcoal) refer to subaerial pyroclastic flows according to Branney and Kokelaar (2002) and phreatomagmatic explosions related to fallout deposits without evidence for long-term water settling conditions.

Stage 3 involves the formation of the 2nd lava dome phase (Fig. 14c), which is the most voluminous part of the TLDF architecture. At the top of the Abaújvár-Telkibánya ignimbrite rests a block and breccia-rich deposit, linked to the renewed dome building events and associated explosive eruptions (column collapse, lateral blasts) or gravity-driven collapse (Peléan or Merapian dome destruction - Heiken and Wohletz, 1987). The emplaced bodies have complex internal textures, and the eroded thickness is

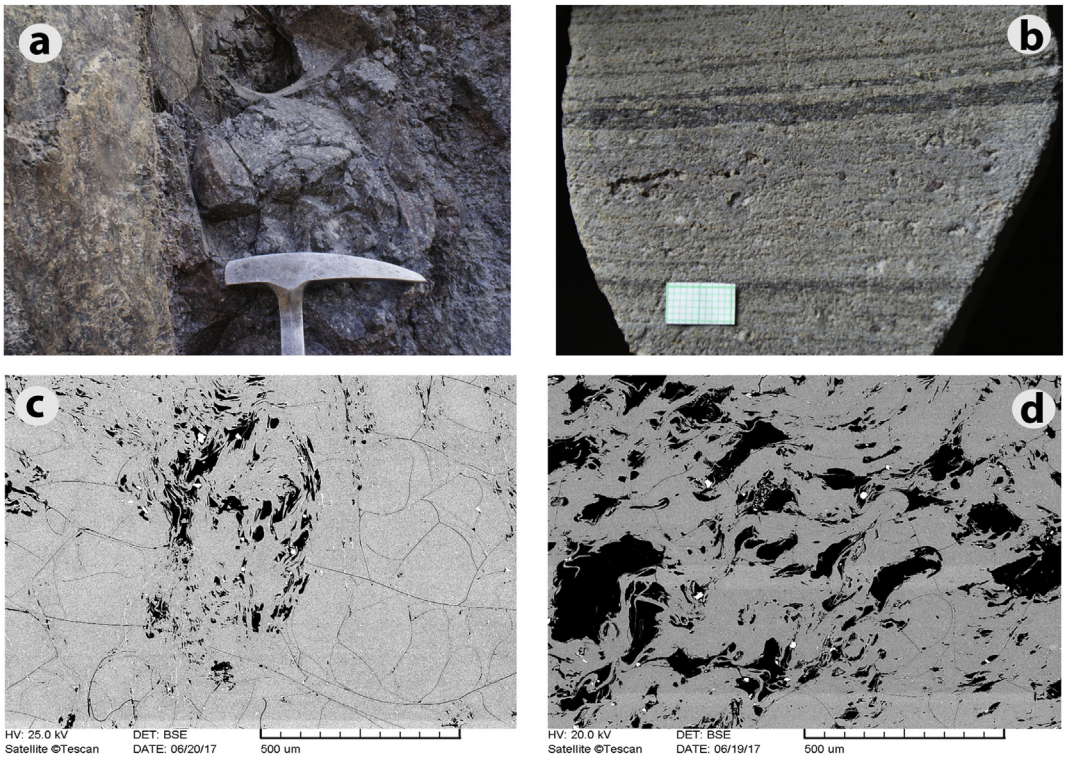

Fig. 8. Textural characteristics of coherent glass (zone f, g) lithofacies association. a) Perlitic glass (zone f) fracturing occurring in different sizes: a larger globular jointed perlite sphere embedding smaller perlite pearls. b) Banded fabric of the pumiceous perlite lithofacies (zone g) at Kőgát Hill. c) Backscattered image of the coherent perlite (zone f) lithofacies showing vesicular and dense glass parts. The longitudinal perlite cracks enclose the smaller, curvy grains. Note that magnetite crystals grow on vesicle rims. d) Backscattered image of the pumiceous perlite lithofacies (zone g) with different vesicle generations: the larger are more equidimensional, while the smaller are stretched vesicles. The coalescence usually occurs along shear planes. Magnetite nucleation on the vesicle rims is also common.

estimated >300 m (Fig. 14d). The geochronology constrained the activity in less than half million years (Fig. 3, Table 2). The only exposed feeder dyke occurrence (Fig. 7f) supports that silicic bodies are usually fed by dykes as reported from Inyo domes (Fink, 1985), Douglas Knob, USA (Befus et al., 2014) and Hrafntinnuhryggur, Iceland (Tuffen and Castro, 2009). The morphology of the lava dome was controlled by the basement topography and by the exogenous or endogenous growth mechanism of the domes (Calder et al., 2015). The thickened (up to 100 m) coherent rhyolite bodies suggest endogenous melt accumulation around the vent as reflected in the shape of erosional forms (coulee, dome). The extensive autoclastic breccia surfaces promote the presence of exogenous growth process forming discrete lobes (2–5 km) from the stretching, highly viscous lava.

The internal lithological variations developed in response to internal temperature gradients, volatile exsolution and hydration, as described by Bonnichsen and Kauffmann (1987) and Sweetkind and Bova (2015), and results in various devitrified, perlitic and fragmental textural types.

The coherent lithofacies associations with devitrified groundmass (zone a-c) indicate that the lava was at elevated temperature above glass transition for prolonged time and thus enabling groundmass crystallization and devitrification (Richnow, 1999; Orth and McPhie, 2003). The superimposed poikilitic, felsitic, spherulitic domains (*zone a*) indicate several different pulses of the melt supply (Manley and Fink, 1987) around the vent. The intensive ductile strain during flow could have resulted in foliated texture (*zone b* Fig. 7a) and folded structures (Figs. 6c, 7b) in compressional zones (Cas and Wright, 1987; Duffield et al., 1995). The subordinate, locally occurred vesiculated microcrystalline lithofacies (*zone c* Fig. 6d) indicates uneven volatile distribution within flow, where the vesiculation is mainly secondary, caused by crystallization of lava interior (Tuffen and Castro, 2009).

The transition zone lithofacies association (*zone d*, *e*) reflects cooling rate differences relative to glass transition, that can be reflected in the dominance of microcrystalline (zone) or glassy groundmass The rarely reported megaspherulites (Silver Cliff, Colorado Smith et al., 2001; Klondyke, Arizona, Simon, 1962; Parana Magmatic Province, Polo et al., 2018) refer to crystallization with sparse nucleation points, thus suggesting highly non-equilibrium conditions (Smith et al., 2001) coupled with locally higher water content (5–7%), lower viscosity and large temperature gradient (ΔT 245–350 °C). The formation of lithophysae rich zones is clear evidence for uneven volatile distribution and locally increased internal vapour pressure (McPhie et al., 1993; Breitkreuz, 2013).

The texture of the coherent glass lithofacies association (*zone f*, *g*) is controlled by lithostatic load, which enabled volatile diffusion to form vesicles only in the shallow, near surface part (0–50 m) of the effusive units. The glassy zones underwent various degrees of hydration resulting perlite. The onion-skin like fracturing formed in function of H_2O diffusion rate, as proposed by Anovitz et al. (2008), Németh et al. (2008) and Denton et al. (2012). The macro scale curvy jointing of dense perlite (Fig. 9a) resembles the quenching-related "macro perlite" jointing described by McPhie et al. (1993). The vesicle sizes and distributions of the pumiceous perlite (*zone g*) indicate multiple bubble nucleation events and that coalescence and stretching were induced by local strain differences in the flow, as proposed by Tuffen and Castro (2009). Magnetite crystallization on vesicle walls could have formed after emplacement during cooling and oxidation of the lava (Fig. 8c, d) like in Rocce Rosse flow, Italy (Shields et al., 2016)

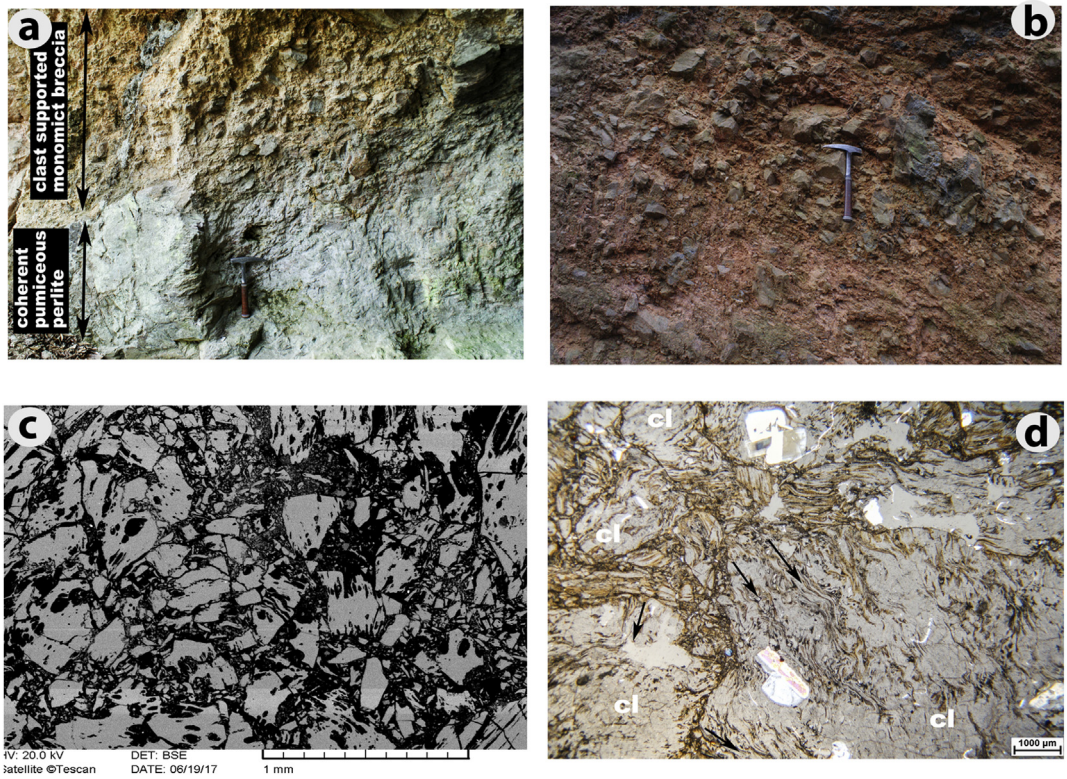

Fig. 9. Textural characteristics of fragmented carapace lithofacies zones (zone h, i). a) Gradual transition between carapace breccia (zone h) and pumiceous perlite (zone g, Templom Hill). b) Typical appearance of the red and black breccia lithofacies (zone, with grey perlite clasts in reddish, pumiceous matrix. The smaller clasts are rotated and aligned around the large perlite block (Varga Hill). c) Backscatterred image of the pumiceous perlite breccia matrix with fine pumiceous clasts (down to ash size). d) Thin section photograph of the red and black breccia lithofacies. The matrix consists of oxidized vesicular glass and phenocryst fragments. The arrows indicate the cracking and vesiculation of obsidian clasts. The borders of larger obsidian like perlite clasts show inflated, vesicular character, while the dense parts are perlitic (Kerek Hill, PPL). (For interpretation of the references to colour in this figure legend, the reader is referred to the web version of this article.)

The textural characteristics of autoclastic lithofacies associations (*zone h–l*) verify the brittle deformation and fragmentation of the coherent zones. The grain size distribution of pumiceous perlite breccia (*zone h*) refers to viscous, blocky flow surface with formation of glass fragments by quench fragmentation (Anderson et al., 1998; Maeno and Taniguchi, 2006). Here, clay alteration of the matrix was probably caused by subsequent weathering under a subtropical Miocene climate (Böhme, 2003). Identified valley confined, clast-supported deposits suggest a gravitational reworking of the dome carapace, which forms a debris accumulation around the dome field, generally thicken downslope and fill the nearby drainage areas (Heiken and Wohletz, 1987).

Reddish breccia zones (*zone i*) are reported from silicic lava flow surfaces by Bonnichsen and Kauffmann (1987), Manley (1996) and Maeno and Taniguchi (2006). Their textural features indicate a unique fragmentation process accompanied by glass fusion and oxidation. The fissure-like geometry and welding-like clast alignment textures could be the result of explosive fragmentation forming explosion pits on the lava surface as a result of local vapour overpressure (Fink and Manley, 1987; Stevenson et al., 1994a; Calder et al., 2015).

Textural characteristics of the other breccia zones (*zone j–l*) are consistent with observations of internal and basal shear zones reported by Bull and McPhie (2007), Smith (1996), Richnow (1999) and Bonnichsen and Kauffmann (1987) for Snake River Plain (USA). The large thickness of the basal breccia layer at Tér Hill (26 m) indicates that continuous advance of the flow resulted in the overriding its own talus apron (Sweetkind and Bova, 2015).

The water content of the glassy and glass bearing lithofacies zones of TLDF are significantly higher (2–5%) than in other cases of younger occurrence. The former interpretation of perlitization (Ilkey-Perlaki and Szöőr, 1973) suggested prolonged post-volcanic water diffusion that caused the perlitic texture. However, this is in contrast with the latest hydration studies (Denton et al., 2012; Aulock et al., 2013) suggesting that diffusion rate is high enough for comprehensive hydration immediately after emplacement between 850 °C and 400 °C (days to month), and much less at ambient temperature. Reported relict obsidian grains in the TSM lavas (Szádeczky, 1887; Lexa et al., 2014;) supports the theory of fast incomplete temperature dependent hydration process. Therefore, we interpret that the hydration pattern of TLDF predominantly reflects post emplacement diffusion of meteoric water (secondary hydration, Giachetti et al., 2015; Seligman et al., 2016) at high diffusion rates, right after or during deposition (Denton et al., 2012; Bindeman and Lowenstern, 2016).

6. Conclusions

The variably uplifted and eroded deposits of the 11.56 ± 0.15 Ma old Miocene Telkibánya Lava Dome Field provide a natural cross section view of these volcanic edifices to study the lithofacies built-up and compare them with younger counterparts. Fieldwork mapping reveals that the stratigraphic architecture of the TLDF is the result of two main dome growth phases (respectively n. 3 and 5 of Fig. 3), with the latter composed of two sub-phases (5a and 5b).

Using the combination of fieldwork based lithofacies analysis at macro- and microscale, we characterized the internal textural heterogeneity of the eroded lava domes and flows. The complex lithofacies architecture contains 12 lithofacies zones grouped in 6 facies associations documenting the layered structural model of obsidian flows. The spatial analysis of the lithofacies occurrence allowed the reconstruction of the original morphology of

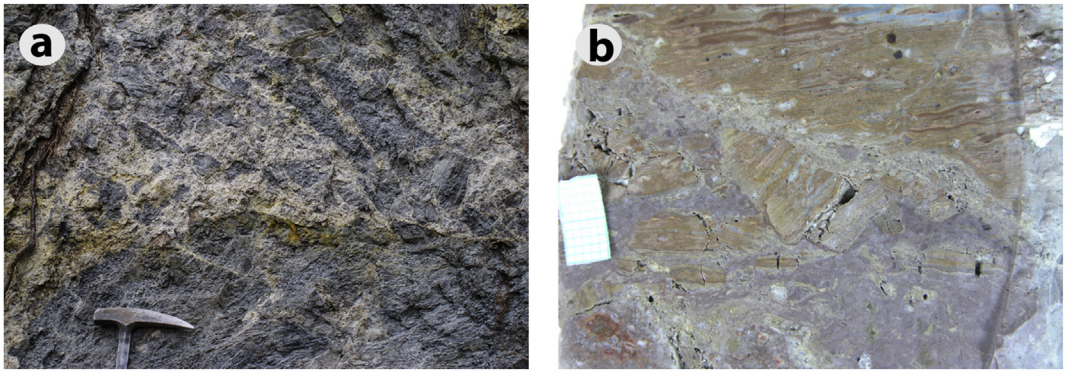

Fig. 10. Textural characteristics of internal breccia zone (zone j, k) (a) clast are closely packed in perlite breccia lithofacies (zone j) showing jig saw fit arrangement, while clast rotation is subordinate, b) internal breccia zone in fluidal microcrystalline rhyolite (zone k), the minor clasts are showing clast alignment around the largest one (top) in the lighter coloured, also microcrystalline matrix.

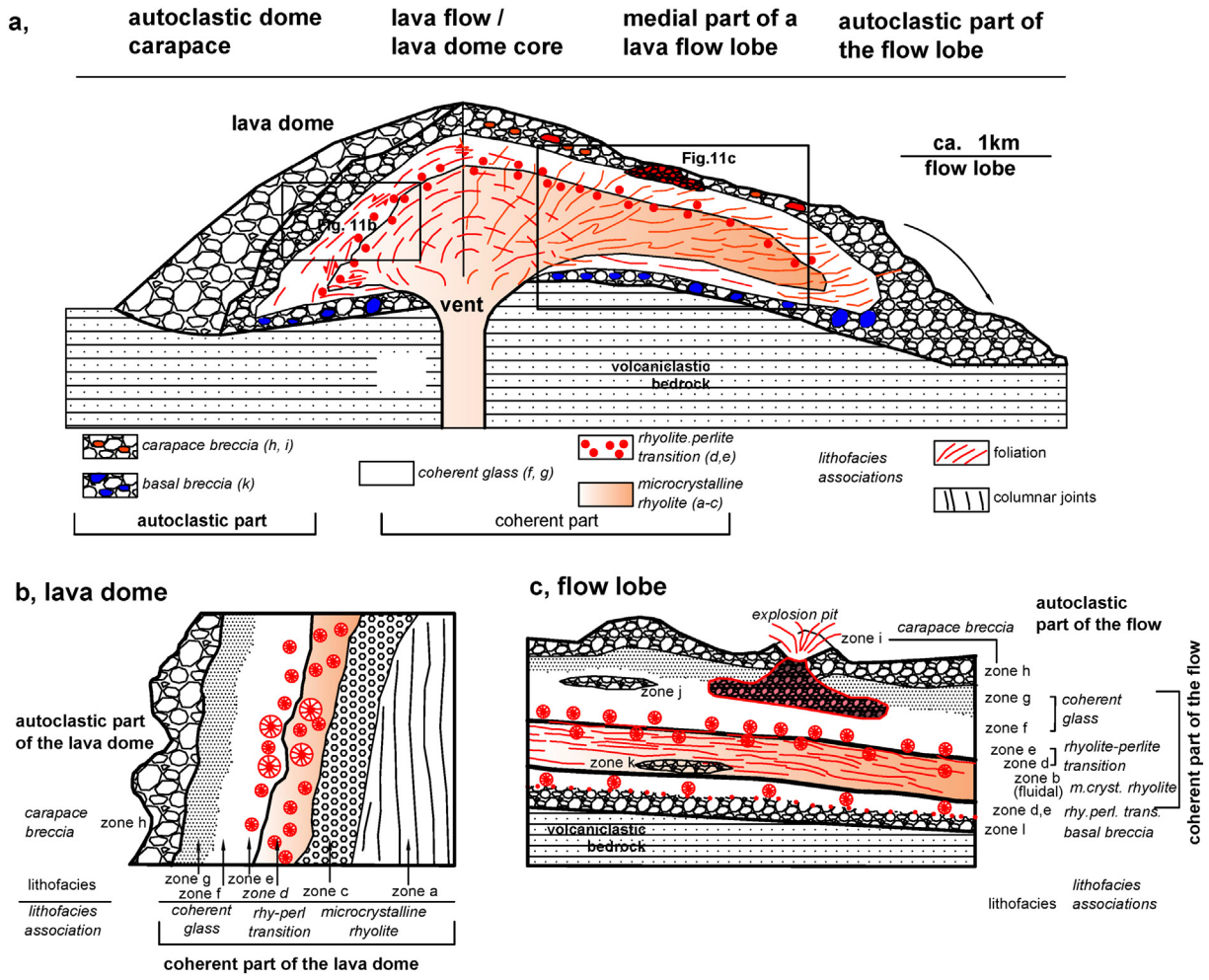

Fig. 11. Lithofacies architecture of a lava flow-dome complex, illustrating the spatial relationships in the textural zonation of Telkibánya Lava Dome Field based on Manley and Fink (1987) and Stevenson et al. (1994a) models. a) Lithofacies associations of a silicic lava flow–dome complex. b) Schematic sketch of lithofacies arrangement at the lava dome's margin. c) Schematic sketch of lithofacies arrangement at the medial part of a flow lobe.

the domes and resulted in the compilation of a lithosomatic map with 5 distinguished edifices in the area. The lithological variability and dome/flow architecture is controlled by several variables including cooling rate, volatile content and degassing which led to crystallization or freezing of the lava interior melt and brittle-ductile fragmentation of the carapace. The textural characteristics of the volcaniclastic and autoclastic lithofacies associations confirm a subaerial setting, but the large amount of the textural water indicates very effective syn- and post-emplacement hydration (up to 5 wt%) by meteoric water.

Acknowledgements

This research has been funded by the Hungarian–Italian MTA-CNR bilateral research project 2016–2018 (led by S. Harangi and G. Groppelli). The research was partly supported by the Hungarian

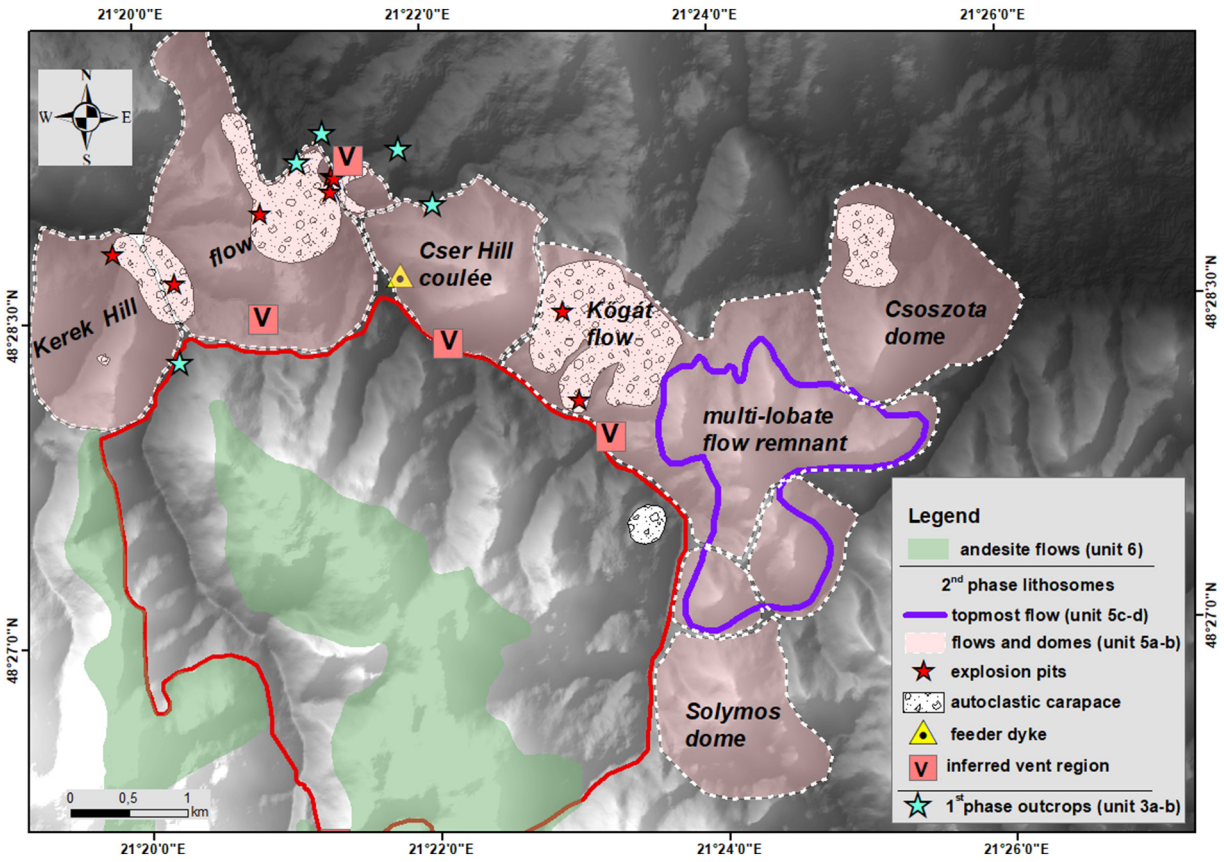

Fig. 12. Distribution of the Telkibánya Lava Dome Field effusive units. The identified lithosomes indicated by white dashed lines.

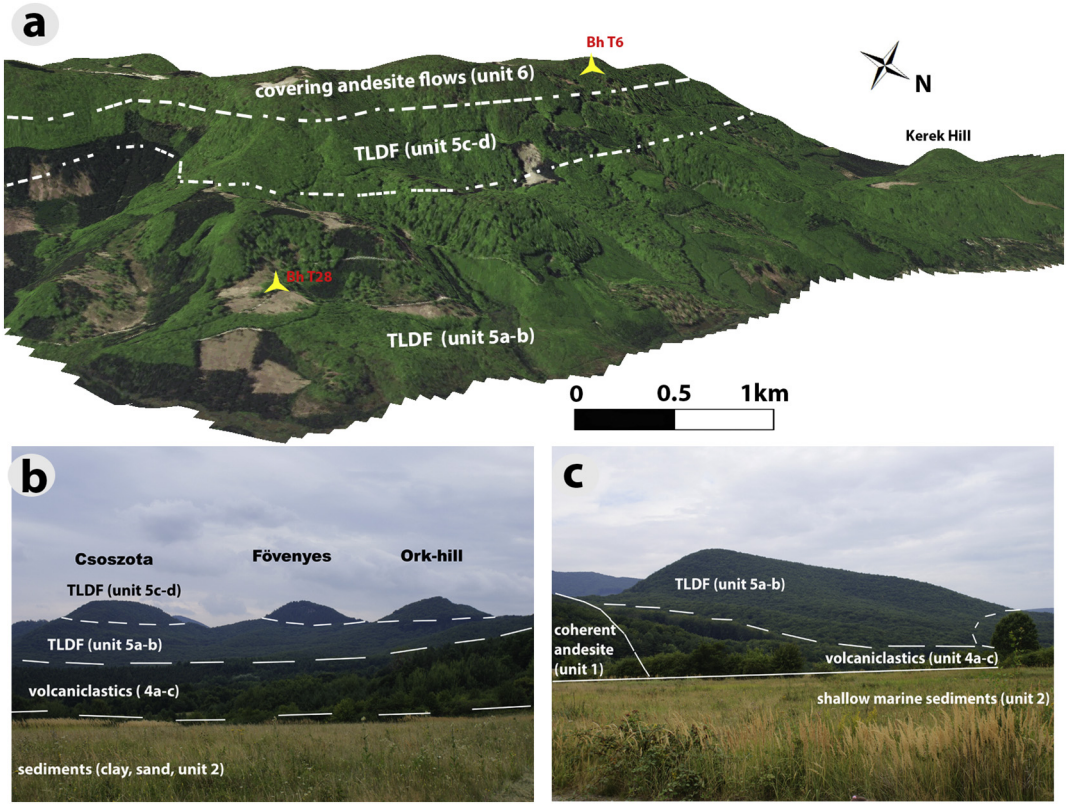

Fig. 13. Morphological features of the Telkibánya Lava Dome Field eroded lava bodies. a) Northeast view of the area covered by andesitic lava flows (Google Earth image on a digital elevation model, SRTM DEM). Uniform steep slopes facing toward the valley. For the stratigraphy of boreholes (T6, T28) see Fig. 5. b) Small eroded cones of the 2nd lava dome phase (view from NW) settled on Abaújvár-Telkibánya ignimbrite succession (NE segment). c) Steep sided coulée of Cser Hill (NE segment).

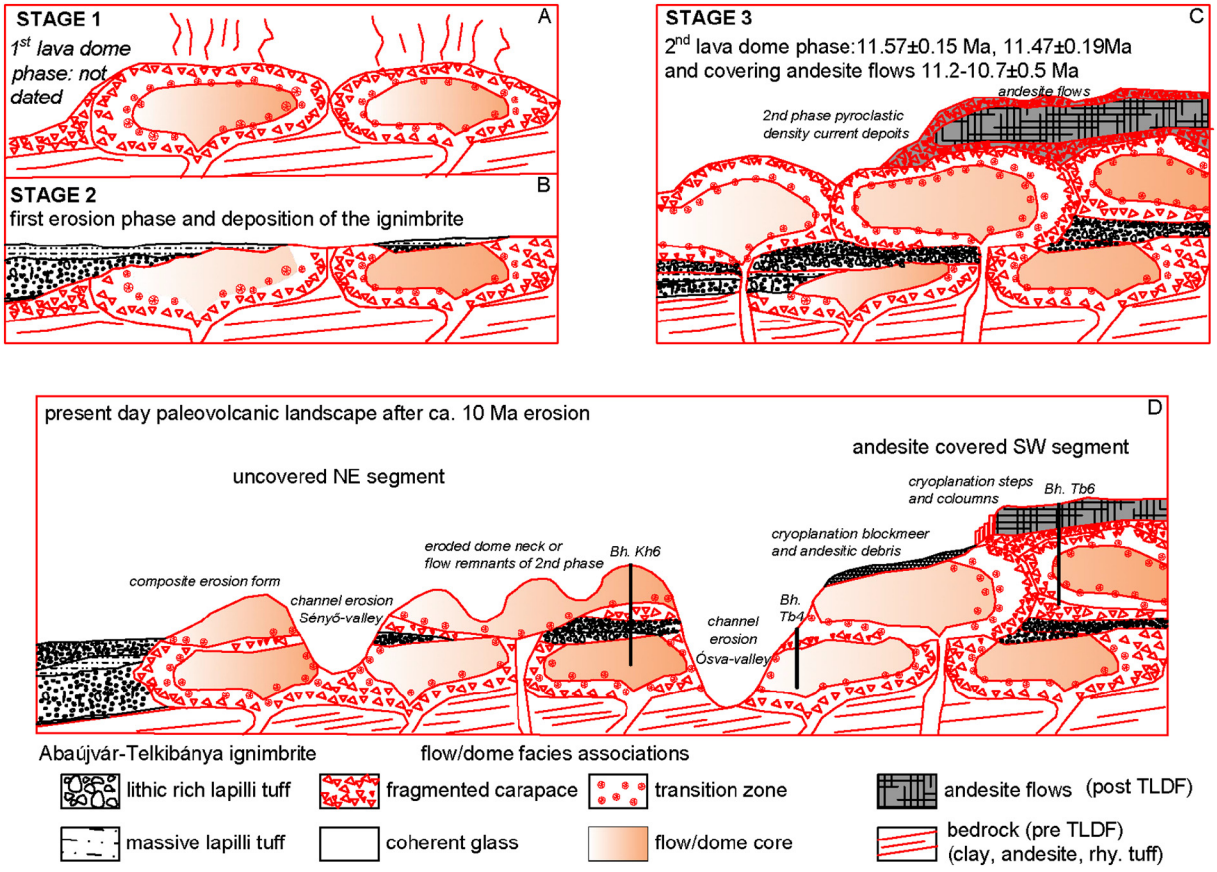

Fig. 14. Sketch of volcanic evolution and erosional phases of the Telkibánya Lava Dome Field.

Scientific Research Fund (PD112584 and PD121048). R.L. and Zs.B. were supported by Bolyai János Research Fellowships. The K/Ar age datings were supported by the European Union and the State of Hungary, co-financed by the European Regional Development Fund in the project of GINOP-2.3.2-15-2016-00009 'ICER'. The authors thank the comments and suggestions made by the guest editor (C. Principe) and two reviewers (Ioan Seghedi and one anonymous) that allowed improving significantly the manuscript.

References

Anderson, S.W., Stofan, E.R., Plaut, J.J., Crown, D.A., 1998. Block size sistribution on silicic lava flow surfaces: implication for emplacement conditions. Geol. Soc. Am. Bull. 110 (10), 1258–1267.

Anovitz, L.M., Cole, D.R., Fayek, M., 2008. Mechanisms of rhyolitic glass hydration below the glass transition. Am. Mineral. 93 (7), 1166–1178, http://dx.doi.org/10.2138/am.2008.2516.

Ashwell, P.A., Kennedy, B.M., Gravley, D.M., von Aulock, F.W., Cole, J.W., 2013. Insights into caldera and regional structures and magma body distribution from lava domes at Rotorua Caldera, New Zealand. J. Volcanol. Geotherm. Res. 258, 187–202.

Aulock, F.W., Nichols, A.R.L., Kennedy, B.M., Oze, C., 2013. Timescales of texture development in a cooling lava dome. Geochim. Cosmochim. Acta 114, 72–80.

Befus, K.S., Zinke, R.W., Jorda, J.S., Manga, M., Gardner, J.E., 2014. Pre-eruptive storage conditions and eruption dynamics of a small rhyolite dome: Douglas Knob, Yellowstone volcanic field, USA. B. Volcanol. 76, 808.

Bindeman, I.N., Lowenstern, J.B., 2016. Low-δD hydration rinds in Yellowstone perlites record rapid syneruptive hydration during glacial and interglacial conditions. Contrib. Mineral. Petrol. 171, 89.

Böhme, M., 2003. The Miocene Climatic Optimum: evidence from ectothermic vertebrates of Central Europe. Palaeo. Geogr. Palaeocl. 195, 389–401.

Bonnichsen, B., Kauffmann, D.F., 1987. Physical features of rhyolite lava flows in the Snake River Plain volcanic province, south-western Idaho. In: Fink, J.H. (Ed.), The Emplacement of Silicic Domes and Lava Flows. Geol. S. Am. S, pp. 119–145.

Bonomo, R., Ricci, V., 2010. Application of the unconformity bounded stratigraphic units (UBSU) to the geological survey of the volcanic island Ustica (Italy). In: Groppelli, G., Viereck-Goette, L. (Eds.), Stratigraphy and Geology of Volcanic Areas: Geol. Soc. Am. S. , pp. 51–61.

Branca, S., Coltelli, M., Groppelli, G., Lentini, F., 2011. Geological map of Etna volcano, 1:50,000 scale. Ital. J. Geosci. 130 (3), 265–291.

Branney, M.J., Kokelaar, B.P., 2002. Pyroclastic density currents and the sedimentation of ignimbrites. Geol. Soc. Mem. 27, 1–152.

Breitkreuz, C., 2013. Spherulites and lithophysae—200 years of investigation on high-temperature crystallization domains in silica-rich volcanic rocks. B. Volcanol. 75, 705.

Bull, K.F., McPhie, J., 2007. Fiamme textures in volcanic successions: flaming issues of definition and interpretation. J. Volcanol. Geotherm. Res. 164, 205–216.

Bullock, L.A., Gertisser, R., O'Driscoll, B., 2018. Emplacement of the Rocche Rosse rhyolite lava flow (Lipari, Aeolian Islands). B. Volcanol. 80, 48.

Calder, E.S., Lavallée, Y., Kendrick, J.E., Bernstein, M., 2015. Lava dome eruptions. In: Sigurdsson, H. (Ed.), The Encyclopedia of Volcanoes. , 2nd ed. Academic Press, pp. 343–362.

Cas, R.A.F., Wright, J.V., 1987. Volcanic Successions, Modern and Ancient. Allen and Unwin, London (528 p).

Cassignol, C., Gillot, P.-Y., 1982. Range and effectiveness of unspiked potassium-argon dating: experimental groundwork and applications. In: Odin, G.S. (Ed.), Numerical Dating in Stratigraphy. Wiley, Chichester, pp. 159–179.

Castro, J., Cashman, K., Joslin, N., Olmsted, B., 2002. Structural origin of large gas cavities in the Big Obsidian Flow, Newberry Volcano. J. Volcanol. Geotherm. Res. 114, 313–330.

Christiansen, R.L., Lipman, P.W., 1966. Emplacement and thermal history of a rhyolite lava flow near Fortymile Canyon, Southern Nevada. Geol. Soc. Am. Bull. 77, 671–684.

Csillag, J., Zelenka, T., 1999. A magyarországi perlit lelőhelyek földtani-genetikai típusai. Építőanyag 51, 34–40.

De Rita, D., Giordano, G., Cecili, A., 2001. A model for sub-marine rhyolite dome growth: Ponza Island (central Italy). J. Volcanol. Geotherm. Res. 107, 221–239.

de Vita, S., Sansivero, F., Orsi, G., Marotta, E., Piochi, M., 2010. Volcanological and structural evolution of the Ischia resurgent caldera (Italy) over the past 10 k.y. In: Groppelli, G., Viereck-Goette, L. (Eds.), Stratigraphy and Geology of Volcanic Areas. Geol. Soc. Am. S, pp. 193–239.

Denton, J., Tuffen, H., Gilbert, J.S., 2012. Variations in hydration within perlitised rhyolitic lavas—evidence from Torfajökull, Iceland. J. Volcanol. Geotherm. Res. 223-224, 64–73.

Dhont, D., Yanev, Y., Bardintzeff, J.M., Chorowicz, J., 2008. Evolution and relationships between volcanism and tectonics in the central-eastern part of the Oligocene Borovitsa caldera (Eastern Rhodopes, Bulgaria). J. Volcanol. Geotherm. Res. 171, 269–286.

Downes, H., Pantó, G., Póka, T., Mattey, D., Greenwood, B., 1995. Calcalkaline volcanics of the Inner Carpathian arc, Northern Hungary: new geochemical and oxygen isotopic results. In: Downes, H., Vaselli, O. (Eds.), Neogene and Related Magmatism in the Carpatho-Pannonian Region: Ac. Vulcanol. , pp. 29–41.

Duffield, W.A., Richter D.H. and Priest S. S., 1995. Physical volcanology of silicic lava domes as exemplified by the Taylor Creek rhyolite, Catron and Sierra counties, New Mexico. US Geological Survey Map I-2399, 1:50,000. 1–16.

Fink, J.H., 1983. Structure and emplacement of a Rhyolite Obsidian Flow: Little Glass Mountain, Medicine Lake Highland, Northern California. Geol. Soc. Am. Bull. 94, 362–380.

Fink, J.H., 1985. Geometry of silicic dikes beneath the Inyo Domes, California. J. Geophys. Res. 90, 11127–11133.

Fink, J.H., Manley, C.R., 1987. Origin of pumiceous and glassy textures in rhyolite domes and flows in the emplacement of silicic domes and lava flows. Geol. Soc. Am. Spec. Pap. 212, 77–89.

Fink, J.H., Anderson, S.W., Manley, C.R., 1992. Textural constraints on effusive silicic volcanism: beyond the permeable foam model. J. Geophys. Res. 97, 9073.

Fodor, L., Csontos, L., Bada, G., Györfi, I., Benkovics, L., 1999. Tertiary tectonic evolution of the Pannonian basin system and neighbouring orogens: a new synthesis of paleostress data. In: Durand, B., Jolivet, L., Horváth, F., Séranne, M. (Eds.), The Mediterranean Basins: Tertiary Extension Within the Alpine Orogen. Geol. Soc. Sp. , pp. 295–334.

García Sánchez, L., Macías, J.L., Sulpizio, R., Osorio-Ocampo, L.S., Pellicioli, C., Pola, A., Avellan, D.R., Cisneros, G., García, F., Ocampo-Díaz, Y.Z.E., Lira-Beltran, R.M., Saucedo, R., Sánchez-Núñez, J.M., Arce, J.L., Corona-Chávez, P., Reyes-Agustin, G., Cardona, M., Layer, P.W., Benowitz, J., Solari, L., Groppelli G., 2019 Geology of La Reforma caldera complex, Baja California, Mexico J Maps (accepted manuscript).

Giachetti, T., Gonnermann, H.M., Gardner, J.E., Shea, T., Gouldstone, A., 2015. Discriminating secondary from magmatic water in rhyolitic matrix-glass of volcanic pyroclasts using thermogravimetric analysis. Geochim. et Cosmochim. Ac. 148, 457–476.

Gillot, P.Y., Cornette, Y., 1986. The Cassignol technique for Potassium-Argon dating, precision and accuracy: examples from the late Pleistocene to recent volcanics from Southern Italy. Chem. Geol. 59, 205–222.

Groppelli, G., Martí, J.,2013. Volcanic stratigraphy – state of the art. In: Proceedings of STRATI 2013, First International Congress on Stratigraphy. Ciências de la Terra (UNL), Lisboa, pp. 99–104.

Gyarmati, P., 1977. A Tokaji-hegység intermedier vulkanizmusa. Annals of the Hungarian Geological Institute 55, 1–195 (in Hungarian).

Gyarmati, P., 1981. Tokaji-hegységi perlitprognózis Összefoglaló jelentés az 1978–80 között elvégzett munkáról. Min. Geol. Surv. Hung. No. 9476 (in Hungarian).

Heiken, G., Wohletz, K., 1987. Tephra deposits associated with silicic domes and lava flows. In: Fink, J.H. (Ed.), The Emplacement of Silicic Domes and Lava Flows. Geol. S. of Am. S. , pp. 55–77.

Hildreth, W., 2004. Volcanological perspectives on Long Valley, Mammoth Mountain and Mono Craters: several contiguous but discrete systems. J. Volcanol. Geoth. Res. 136, 169–198.

Ilkey-Perlaki, E., 1967. Gönc. Magyarázó a Tokaji-hegység földtani térképéhez, 25000-es sorozat. Hung. Geol. Inst., 1–48 (in Hungarian).

Ilkey-Perlaki, E., 1971. Gönc. A Tokaji-hegység földtani térképe 1:25000. Hung. Geol. Inst (in Hungarian).

Ilkey-Perlaki, E., 1972. A Telkibánya – Kőgát-i perliteľofordulás felderíťő kutatásának zárójelentése és készletszámítása. Min. Geol. Surv. Hung., 1–311 (in Hungarian).

Ilkey-Perlaki, E., 1977. Nyíri. A Tokaji-hegység földtani térképe 1:25000. Hung. Geol. Inst (in Hungarian).

Ilkey-Perlaki, E., 1978. Nyíri. Magyarázó a Tokaji-hegység földtani térképéhez, 25000-es sorozat. Hung. Geol. Inst., 1–55.

Ilkey-Perlaki, E., Szöör, Gy, 1973. The perlites of the Tokaj Moutains. Acta Geol. Ac. Sci. Hung. 17 (1–3), 85–106.

Kaličiak, M.I., Žec, B., 1995. Review of Neogene volcanism of Eastern Slovakia. Ac.Volcanol. 7, 87–95.

Kiss, J., Zelenka, T., 2009. Geological features, geophysical measurements and interpretation at the Telkibánya research area. Telkibánya Geology Publ. Univ. Miskolc, Ser. A Min. 78, 97–115.

Kiss, P., Gméling, K., Molnár, F., Pécskay, Z., 2010. Geochemistry of Sarmatian volcanic rocks in the Tokaj Mts (NE Hungary) and their relationship to hydrothermal mineralization. Cent. Eur. Geol. 53, 377–403.

Kováč, M., Andreyeva-Grigorovich, A., Bajraktarević, Z., Brzobohatý, R., Filipescu, S., Fodor, L., Harzhauser, M., Nagymarosy, A., Oszczypko, N., Pavelić, D., Rögl, F., Saftić, B., Sliva, Ľ., Studencka, B., 2007. Badenian evolution of the Central Paratethys Sea: paleogeography, climate and eustatic sea-level changes. Geol. Carp. 58, 579–606.

Kováč, M., Halásová, E., Hudáčková, N., Holcová, K., Hyžný, M., Jamrich, M., Ruman, R., 2018. Towards better correlation of the Central Paratethys regional time scale with the standard geological time scale of the Miocene Epoch. Geol. Carpath. 69, 283–300.

Lexa, J., Seghedi, I., Németh, K., Szakács, A., Konecný, V., Pécskay, Z., Fülöp, A., Kovacs, M., 2010. Neogene-Quaternary Volcanic forms in the Carpathian-Pannonian Region: a review. Cent. Eur. J. Geosc. 2, 207–270.

Lexa, J., Baco, P., Bacova, Z., Konecny, P., Konecny, V., Németh, K., Pécskay, Z., 2014. Evolution of monogentic rhyolite volcanoes: Vinicky, Eastern Slovakia. In: Bequiraj, A., Ionescu, C., Christofides, G., Uta, A., Beqiraj Goga, E., Marku, S. (Eds.), Proceedings XX. Congress of the Carpathian – Balkan Geological Association Bul. Shk. Gjeol. Special Issue. , pp. 234–237.

Lucchi, F., 2013. Stratigraphic methodology for the geological mapping of volcanic areas: insights from the Aeolian archipelago (southern Italy). Geol Soc Mem Aeolian Islands Volcanoes 37, 37–53.

Maeno, F., Taniguchi, H., 2006. Silicic lava dome growth in the 1934–1935 Showa Iwo-jima eruption, Kikai caldera, south of Kyushu, Japan. B. Volcanol. 68, 673–688.

Manley, C.R., 1996. Physical volcanology of a voluminous rhyolite lava flow: The Badlands lava, Owyhee Plateau, southwestern Idaho. J. Volcanol. Geotherm. Res. 71 (2–4), 129–153, http://dx.doi.org/10.1016/0377-0273(95)00066-6.

Manley, C.R., Fink, J.H., 1987. Internal textures of rhyolite flows as revealed by research drilling. Geology 15, 549–555.

Martí, J., Groppelli, G., Brum da Silveira, A., 2018. Volcanic stratigraphy: a review. J. Volcanol. Geotherm. Res. 357, 68–91.

McPhie, J., Doyle, M., Allen, R., 1993. Volcanic Textures; A Guide to the Interpretation of Textures in Volcanic Rocks. University of Tasmania, pp. 1–196.

Molnár, F., Zelenka, T., Pécskay, Z., 2009. Geology, Styles of Mineralization and Spatial-Temporal Characteristics of the Hydrothermal System in the Low Suphidation-Type Epithermal Gold-Silver Deposit at Telkibánya Publ. Univ. Miskolc, Ser. A, min., pp. 45–71.

Németh, K., Pécskay, Z., Martin, U., Gméling, K., Molnár, F., Cronin, S.J., 2008. Hyaloclastites, peperites and soft-sediment deformation textures of a shallow subaquaeous Miocene rhyolitic dome-cryptodome complex, Pálháza, Hungary. Geol. Soc. Spec. Publ. 302, 63–86.

Orth, K., McPhie, J., 2003. Textures formed during emplacement and cooling of a Plateoproterozoic, small-volume rhyolitic sill. J. Volcanol. Geoth. Res. 128, 341–362.

Pasquarè, G., Abbate, E., Bosi, C., Castiglioni, G.B., Merenda, L., Mutti, E., Orombelli, G., Ortolani, F., Parlotto, M., Pignone, R., Polino, R., Premoli Silva, E., Sassi, F.P., 1992. Guida al Rilevamento della Nuova Carta Geologica d'Italia: Rome, Servizio Geologico Nazionale. Quaderni Serie III 1, 1–203.

Pécskay, Z., Molnár, F., 2002. Relationships between volcanism and hidrotermal activity in the Tokaj Mountains, Northeast Hungary. Geol. Carp. 53, 303–314.

Pécskay, Z., Balogh, K., Székyné, F.V., Gyarmati, P., 1987. A Tokaji-hegység miocén vulkánosságának K/Ar geokronológiája Földt. Közl 117, 237–253.

Pécskay, Z., Lexa, J., Szakács, A., Balogh, K., Seghedi, I., Konecný, V., Kovác, M., Márton, E., Széky- Fux, V., Póka, T., Gyarmati, P., Edelstein, O., Rosu, E., Zec, B., 1995. Space and time distribution of Neogene–Quaternary volcanism in the Carpatho-Pannonian region. Acta Vulcanol. 7, 15–29.

Pécskay, Z., Lexa, J., Szakács, A., Seghedi, I., Balogh, K., Konečný, V., Zelenka, T., Kovacs, M., Póka, T., Fülöp, A., Márton, E., Panaiotu, C., Cvetković, V., 2006. Geochronology of Neogene–Quaternary magmatism in the Carpathian arc and intra-Carpathian area: a review. Geol. Carp. 57, 511–530.

Petrik, A., Beke, B., Fodor, L., 2014. Combined analysis of faults and deformation bands reveals the Cenozoic structural evolution of the southern Bükk foreland (Hungary). Tectonophysics 633, 43–62.

Piller, W.E., Harzhauser, M., Mandic, O., 2007. Miocene Central Paratethys stratigraphy — current status and future directions. Stratigraphy 4, 151–168.

Polo, L.A., Janasi, V.A., Giordano, D., Lima, E.F., Cañon-Tapia, E., Roverato, M., 2018. Effusive silicic volcanism in the Paraná Magmatic Province, South Brazil evidence for locally-fed lava flows and domes from detailed field work. J. Volcanol. Geotherm. Res. 355, 204–218.

Porreca, M., Cifelli, F., Soriano, C., Giordano, G., Romano, C., Conticelli, S., Mattei, M., 2014. Hyaloclastite fragmentation below the glass transition: An example from El Barronal submarine volcanic complex (Spain). Geology 42 (1), 87–90, http://dx.doi.org/10.1130/G34744.1.

Richnow, J., PhD Thesis 1999. Eruptional and Post-Eruptional Processes in Rhyolite Domes. University of Canterbury, New Zealand, pp. 1–546.

Salvador, A., 1994. International Stratigraphic Guide: A Guide to Stratigraphic Classification, Terminology, and Procedure. The International Union of Geological Sciences and the Geological Society of America, Boulder, Colorado (214 p).

Seghedi, I., 2011. Permian rhyolitic volcanism, changing from subaqueous to subaerial in post-Variscan intra-continental Sirinia Basin (SW Romania–Eastern Europe). J. Volcanol. Geoth. Res. 201, 312–324.

Seligman, A.N., Bindeman, I.N., Watkins, J.M., Ross, A.M., 2016. Water in volcanic glass: from volcanic degassing to secondary hydration. Geochim. Cosmochim. Acta 191, 216–238.

Shields, J.K., Mader, H.M., Caricchi, L., Tuffen, H.S., Pistone, M., Baumgartner, L., 2016. Unravelling textural heterogeneity in obsidian: Shear-induced outgassing in the Rocche Rosse flow. J. Volcanol. Geoth. Res. 310, 137–158.

Simon, F.S., 1962. Devitrification dikes and giant spherulites from Klondyke, Arizona. Am. Mineral. 47, 871–885.

Smith, J.V., 1996. Ductile-brittle transition structures in the basal shear zone of a rhyolite lava flow, eastern Australia. J. Volcanol. Geoth. Res. 72, 217–223.

Smith, R.K., Tremallo, R.L., Lofgren, G.E., 2001. Growth of megaspherulites in a rhyolitic vitrophyre. Am. Mineral. 86, 589–600.

Steiger, R.H., Jager, E., 1977. Subcommission on geochronology; Convention on the use of decay constants in geo- and cosmochronology. Earth Plan. Sci. Lett. 36, 359–362.

Stevenson, R.J., Briggs, R.M., Hodder, A.P.W., 1994a. Physical volcanology and emplacement history of the Ben Lomond rhyolite lava flow, Taupo Volcanic Centre, New Zealand. New Zeal. J. Geol. Geop. 37, 345–358.

Stevenson, R.J., Hodder, A.P.W., Briggs, R.M., 1994b. Rheological estimates of rhyolite lava flows from Okataina Volcanic Centre, New Zealand. New Zeal. J. Geol. Geop. 37, 211–221.

Sweetkind, D.S., Bova, S.C., 2015. Field-based description of rhyolite lava flows of the Calico Hills Formation, Nevada National Security Site, Nevada. Sci. Investig. Rep., 46.

Szádeczky, Gy, 1887. A magyarországi obsidianok, különös tekintettel geológiai viszonyaikra. Értekezések a Term. Tud. Köréből 16, 1–64 (in Hungarian).
Szentgyörgyi, K., 1978. The Sarmatian formations in the Tiszántúl area (East Hungary) and their stratigraphic position. Acta Miner. Petro., Szeged 23 (2), 279–297.
Szepesi, J., 2009. Geology of the rhyolite-perlite extrusions along Ósva-valley, Telkibánya. Telkibánya Geology Publ. Univ. Miskolc, Ser. A, Min. 78, 171–193.
Tuffen, H., Castro, J., 2009. The emplacement of an obsidian dyke through thin ice: Hrafntinnuhryggur, Krafla Iceland. J. Volcanol. Geoth. Res. 185, 352–366.
Tuffen, H., James, M.R., Castro, J.M., Schipper, C.I., 2013. Exceptional mobility of an advancing rhyolitic obsidian flow at Cordón Caulle volcano in Chile. Nat. Commun. 4, 1–7.
Wheeler, H.E., Mallory, V.S., 1953. Designation of stratigraphic units. AAPG Bull. 37, 2407–2421.
Zelenka, T., 2013. Geology of the perlite bodies at Pálháza 19–21. European Geologist 36, 19–21.
Zelenka, T., Gyarmati, P., Kiss, 2012. Paleovolcanic reconstruction in the Tokaj Mountains Cent. Eur. Geol 55, 49–84.